

The Molecular Interstellar Medium in Ultraluminous Infrared Galaxies

P. M. Solomon

Astronomy Program, State University of New York, Stony Brook, NY 11794

D. Downes

Institut de Radio Astronomie Millimétrique, 38406 St. Martin d'Hères, France

S. J. E. Radford

National Radio Astronomy Observatory, Tucson AZ 85721

and

J. W. Barrett

Astronomy Program, State University of New York, Stony Brook, NY 11794

Received March 28, 1996; accepted _____

ABSTRACT

We present observations with the IRAM 30 m telescope of CO in a large sample of ultraluminous IR galaxies out to redshift $z = 0.3$. Most of the ultraluminous galaxies in this sample are interacting, but not completed mergers. The CO(1–0) luminosity of all but one of the ultraluminous galaxies is high, with values of $\log(L'_{\text{CO}}/\text{K km s}^{-1} \text{ pc}^2) = 9.92 \pm 0.12$. The extremely small dispersion of only 30 % is less than that of the far infrared luminosity. The integrated CO line intensity is strongly correlated with the $100 \mu\text{m}$ flux density, as expected for a black body model in which the mid and far IR radiation is optically thick. We use this model to derive sizes of the FIR and CO emitting regions and the enclosed dynamical masses. Both the IR and CO emission originate in regions a few hundred parsecs in radius. The median value of $L_{\text{FIR}}/L'_{\text{CO}} = 160 \text{ L}_\odot/\text{K km s}^{-1} \text{ pc}^2$, within a factor of two or three of the black body limit for the observed far IR temperatures. The entire ISM is a scaled up version of a normal galactic disk with the ambient densities a factor of 100 higher, making even the intercloud medium a molecular region. We compare three different techniques of H_2 mass estimation and conclude that the ratio of gas mass to CO luminosity is about a factor of four times lower than for Galactic molecular clouds, but that the gas mass is a large fraction of the dynamical mass. Our analysis of CO emission from ultraluminous galaxies reduces the H_2 mass from previous estimates of $2 - 5 \times 10^{10} \text{ M}_\odot$ to $0.4 - 1.5 \times 10^{10} \text{ M}_\odot$, which is in the range found for molecular gas rich spiral galaxies. A collision involving a molecular gas rich spiral could lead to an ultraluminous galaxy powered by central starbursts triggered by the compression of infalling preexisting GMC's.

The extremely dense molecular gas in the center of an ultraluminous galaxy is an ideal stellar nursery for a huge starburst.

Subject headings: galaxies: nuclei — galaxies: interstellar matter — galaxies: starburst — galaxies: ISM: dust, extinction — radio lines: galaxies — infrared: galaxies

1. INTRODUCTION: A NEW CO STUDY OF ULTRALUMINOUS GALAXIES

We report here an observational study of the molecular content of a large sample of extremely luminous infrared galaxies. Ultraluminous galaxies, those with IR luminosities¹ $> 10^{12} L_\odot$ (cf. Wright, Joseph and Meikle, 1984; Sanders et al. 1988a), are the most luminous objects in the local universe. They typically radiate 90% or more of their energy in the far infrared. Most of these objects were discovered by the IRAS survey and many were previously uncatalogued. All ten of the brightest (nearest) ultraluminous galaxies (Sanders et al. 1988a) are either merging systems or have tidal tails indicating a recent merger. Besides the very large IR luminosity, the molecular interstellar medium in such galaxies differs from that in normal spiral galaxies in several fundamental respects. First, even though these galaxies have high CO luminosities and molecular masses, the ratio of far infrared to CO luminosity is about an order of magnitude greater than for normal spiral galaxies (e.g., Sanders et al. 1986; Solomon & Sage 1988). In star formation models, this implies a much higher star formation rate per Solar mass of molecular gas than in normal galaxies, even gas rich spirals. Second, a large fraction of their molecular gas is at densities much higher than in ordinary giant molecular clouds, as shown by HCN observations which trace gas at densities $> 10^5 \text{ cm}^{-3}$ (Solomon, Downes, & Radford 1992a). Third, direct interferometric measurements of nearby ultraluminous galaxies (e.g., Scoville et al. 1991; Radford et al. 1991b) show most of the CO, HCN, and molecular mass is concentrated in a small central region (less than 1 kpc). Indeed, estimates of the molecular mass in the central condensation often equal the dynamical mass (e.g., Scoville et al. 1991). This conflict between dynamical mass and H₂ mass derived from CO luminosity leads to a new interpretation of the CO luminosity (Downes, Solomon, & Radford 1993; hereafter DSR) for a medium which may fill a disk or sphere in the central few hundred parsecs of a galaxy.

In this paper we present the results of a systematic CO(1–0) survey with the IRAM 30 m telescope of a large sample of ultraluminous galaxies out to $z = 0.27$. This is part of a multiline study with a goal of understanding the difference between the star-forming environment in ultraluminous galaxies and large spiral galaxies. The observational data are in section 2. We derive CO and IR luminosities and temperatures in section 3 and compare them with the values for normal spirals. We have previously suggested that for the extreme conditions of ultraluminous galaxies, the ratio of IR to CO luminosity approaches the ratio expected for a black body (DSR). This implies the dust is optically thick even at far IR wavelengths (see also Condon et al. 1991) and the ratio is not a simple indicator of luminosity to molecular mass. In section 4, we review the black body model and discuss

¹ We use $H_0 = 75 \text{ km s}^{-1} \text{ Mpc}^{-1}$ and $q_0 = 0.5$ throughout this paper.

the validity of our black-body approximation for the central regions. In section 5, we derive the dynamical mass from the model and the observations, and compare it with the H₂ mass derived from CO luminosity. We also derive a lower limit to the molecular mass by assuming the CO is optically thin, and we compare the mass calculated by different approximations. We discuss the limits of the model, the extent to which gas may be a dominant part of the dynamical mass in the centers of these galaxies and the implications for the nature of the luminosity source.

2. OBSERVATIONS

2.1. The Sample and Observing Methods

2.1.1. Source Selection

The sample contains 37 infrared luminous galaxies in the redshift range $z = 0.03$ to 0.27 . Of these 11, including the well known sources Arp 220 and Mrk 231, have $60\text{ }\mu\text{m}$ fluxes $S_{60} > 5.0$ Jy and are part of the nearby bright galaxy sample (Sanders et al. 1988a; Sanders, Scoville, & Soifer 1991). They have previously been observed in CO by several groups. Twenty galaxies were chosen from a redshift survey (Strauss et al. 1992) of all IRAS sources with $60\text{ }\mu\text{m}$ fluxes $S_{60} > 1.9$ Jy. We selected primarily the most far infrared luminous sources (see equation 4) at $\delta > -10^\circ$; a few lower luminosity sources were also included. We excluded a few sources from the redshift survey whose unrealistically high $100/60\text{ }\mu\text{m}$ flux ratios indicate they are probably contaminated by Galactic emission. In order to include more galaxies at very high infrared luminosity we also observed 7 sources with $60\text{ }\mu\text{m}$ fluxes between 1.2 and 1.9 Jy from the extension of the redshift survey. (Fisher et al., 1995) These are the most distant, $0.15 \leq z \leq 0.27$, galaxies in the sample.

Although not complete, our sample includes a large fraction of the most luminous IRAS galaxies in the northern sky. Of the ten most luminous galaxies in the redshift survey above $\delta > -10^\circ$, our sample includes eight. One of the missing sources is the radio-loud quasar 3C273. Twenty galaxies in our sample are more luminous than the prototype IR galaxy Arp 220 and 25 have a far infrared luminosity, $L_{\text{FIR}} > 1 \times 10^{12} L_\odot$, obtained from the color corrected 60 and $100\text{ }\mu\text{m}$ flux (see equation 4). The most luminous object in the sample, 14070+0525, with $4 \times 10^{12} L_\odot$ in the far IR, is also the most distant.

In our sample, the mean far IR color $S_{60}/S_{100} = 0.81$, is slightly cooler than in the smaller sample studied by Sanders et al. (1988a), where the mean $S_{60}/S_{100} = 0.93$ (Sanders, private communication). Only 19% of the galaxies in our sample have $S_{60}/S_{100} > 1.0$,

while 50% have $S_{60}/S_{100} > 1.0$ in Sanders et al.’s sample. A possible explanation is that although most of our sample was taken from a redshift survey of 60 μm sources, we selected candidates based on total far infrared luminosity including the contribution from 100 μm . The sample covers higher redshifts than the earlier studies (Sanders et al. 1988a; 1991). **Figure 1** shows the redshift distribution for the galaxies described here, which extends to $cz = 80000 \text{ km s}^{-1}$. For comparison, Sanders, et al. (1991) included three ultraluminous galaxies in their highest range of redshift, $cz = 15000 - 25000 \text{ km s}^{-1}$. In the redshift range $cz = 15000 - 80000 \text{ km s}^{-1}$, our sample has 25 galaxies with 60 μm fluxes between 1.0 and 5 Jy. Of these, 22 galaxies have a FIR luminosity $L_{\text{FIR}} > 1 \times 10^{12} \text{ L}_{\odot}$.

2.1.2. Positions of the IRAS Galaxies

With the IRAM 30 m telescope, which has a beamwidth of 22" at 115 GHz and 13" at 230 GHz, CO observations require source positions accurate to a few arcsec. This is more accurate than positions in the IRAS catalogs (Moshir et al. 1992; Beichman et al. 1988), which typically have error ellipses with major axes of 15" – 20". For the faintest sources, the IRAS positions may be no better than 30". Hence we determined positions of candidate galaxies near the center of the IRAS error ellipse for each source from the Palomar Sky Survey prints with a measuring engine. The weakest sources have visual magnitudes near the Sky Survey limit (mag 17 to 18). We could usually identify the most likely galaxy by inspection and we detected CO in all of these with no exceptions. **Table 1** gives the positions where we detected CO. We estimate the accuracy to be $\pm 3''$ for sources with positions from the Sky Survey. For a few of the stronger sources we used VLA continuum positions (Condon et al. 1991).

Some potential sources selected from the extension to the redshift survey with 60 μm fluxes between 1.2 and 1.9 Jy are in confused fields where we found several very faint candidates. In 5 cases we stopped looking after one or two tries due to limited observing time. The limits in these cases were not low enough to be interesting given the very weak far IR flux. In other words we simply did not invest the observing time required to reach the expected integrated intensity given the low 100 μm flux (see Fig. 4, section 4), and the confused position. These sources are not included in the sample.

2.1.3. CO Observations

The CO observations were made with the IRAM 30 m telescope on Pico Veleta near Granada, Spain. All observations were done with a wobbling secondary with a throw of 120"

– 240" in a double switching mode, alternating on–off and off–on. The SIS receivers had typical SSB noise temperatures of 130 – 230 K. The 512×1 MHz filter banks covered 1400 – 1600 km s^{-1} at the redshifted CO(1–0) line and the data were smoothed to resolutions of 8 MHz ($\approx 24 \text{ km s}^{-1}$) or 16 MHz ($\approx 48 \text{ km s}^{-1}$) for analysis. To test the reality of the weakest lines, we used two local oscillator settings, shifting the lines by 200 – 300 km s^{-1} . The data were calibrated with cold and ambient loads and pointing was checked on planets and quasars. Atmospheric opacities were typically < 0.1 at the observing frequencies of 91 – 110 GHz. At these frequencies, the telescope's forward efficiency is 90% and its main beam efficiency is 60%. In this paper, spectra and intensities, I_{CO} , are in main beam brightness temperature, T_{mb} , which is appropriate for small sources. For the 30 m telescope, $T_{\text{mb}} = 1 \text{ K}$ corresponds to a flux density of 4.5 Jy from a point source in the 3mm band.

Spectra of the sources are shown in **Fig. 2** and integrated intensities are listed in **Table 1**. A few of these spectra have been published previously (Radford, Solomon & Downes 1991a; Solomon, Downes & Radford 1992a). The peak intensities range from $T_{\text{mb}} = 2 \text{ mK}$ for the most distant object at $z = 0.265$ to $\sim 100 \text{ mK}$ for the nearest sources. The CO redshifts agree well with the optical redshifts; the difference between the two is typically $\leq 30 \text{ km s}^{-1}$. The linewidths in **Table 1** are either the full width at half maximum of Gaussian fits or one-half the full width to zero intensity for line profiles that are strongly non-gaussian. Unlike spectra from normal spirals, many of these profiles are centrally peaked.

In addition to CO data, we present R-band CCD images of 12 of the galaxies between RA 10h and 23h, taken at the University of Hawaii 2.2 m telescope. The galaxy morphology shown by these images is discussed in Section 6; for easy reference, we place our CO spectra next to the images in order of decreasing redshift (**Fig. 7**).

3. CO AND INFRARED LUMINOSITIES

Table 2 lists the CO and far IR luminosities of the sample galaxies. Here we describe how we calculate luminosities from observed fluxes and we compare the luminosities with those of normal galaxies.

3.1. CO Luminosities

3.1.1. Basic Expressions

The CO line luminosity can be expressed several ways. Monochromatic luminosity $L(\nu_{\text{rest}})$, observed flux density $S(\nu_{\text{obs}})$, and luminosity distance D_L are related by $\nu_{\text{rest}} L(\nu_{\text{rest}}) = 4\pi D_L^2 \nu_{\text{obs}} S(\nu_{\text{obs}})$, so

$$L_{\text{CO}} = 1.04 \times 10^{-3} S_{\text{CO}} \Delta V \nu_{\text{rest}} (1+z)^{-1} D_L^2 , \quad (1)$$

where L_{CO} is the CO line luminosity in L_\odot , $S_{\text{CO}} \Delta V$ is the velocity integrated flux in Jy km s^{-1} , $\nu_{\text{rest}} = \nu_{\text{obs}}(1+z)$ is the rest frequency in GHz, and D_L is the luminosity distance in Mpc.

Often CO line luminosity is expressed as velocity integrated source brightness temperature, $T_b \Delta V$, times source area, $\Omega_s D_A^2$, where Ω_s is the solid angle subtended by the source and $D_A = D_L/(1+z)^2$ is the angular size distance. The observed integrated line intensity, $I_{\text{CO}} = \int T_{\text{mb}} dV$, is obtained from the beam-diluted brightness temperature. This must be corrected for redshift to get the intrinsic source brightness temperature, $T_b \Delta V \Omega_s = I_{\text{CO}} \Omega_{\text{s*}}(1+z)$, where $\Omega_{\text{s*}}$ is the solid angle of the source convolved with the telescope beam. Then the line luminosity $L'_{\text{CO}} = T_b \Delta V \Omega_s D_A^2 = \Omega_{\text{s*}} D_L^2 I_{\text{CO}}(1+z)^{-3}$, or

$$L'_{\text{CO}} = 23.5 \Omega_{\text{s*}} D_L^2 I_{\text{CO}} (1+z)^{-3} \quad (2)$$

when L'_{CO} is in $\text{K km s}^{-1} \text{pc}^2$, $\Omega_{\text{s*}}$ is in arcsec^2 , D_L is in Mpc, and I_{CO} is in K km s^{-1} . If the source is much smaller than the beam, $\Omega_{\text{s*}} \approx \Omega_b$. Here we see that for a fixed beam size and source luminosity, the integrated line intensity does *not* scale as D_L^{-2} , but rather as $(1+z)^3 D_L^{-2}$ (Solomon, Radford, & Downes 1992). The line luminosity, L'_{CO} , can also be expressed for a source of any size in terms of the total line flux, $L'_{\text{CO}} = (c^2/2k) S_{\text{CO}} \Delta V \nu_{\text{obs}}^{-2} D_L^2 (1+z)^{-3}$, or

$$L'_{\text{CO}} = 3.25 \times 10^7 S_{\text{CO}} \Delta V \nu_{\text{obs}}^{-2} D_L^2 (1+z)^{-3} . \quad (3)$$

with $S_{\text{CO}} \Delta V$ in Jy km s^{-1} , ν_{obs} in GHz, and D_L in Mpc.

The quantity L'_{CO} is useful because it is surface brightness times area, in brightness temperature units. Thus two lines with the same T_b and extent will have the same L'_{CO} , regardless of transition or line frequency. Conversely, the L'_{CO} ratio of two lines is the average over the source of the lines' intrinsic T_b ratio, which is an indicator of physical conditions in the gas.

3.1.2. CO Luminosities and Gas Masses for this Sample

Table 2 lists the CO luminosities and the nominal gas masses $M'(\text{H}_2)$ computed with a standard Milky Way H_2 mass-to-CO luminosity ratio of $4.6 \text{ M}_\odot/\text{K km s}^{-1} \text{ pc}^2$ (Solomon

et al. 1987). The average for the sample is $L'_{\text{CO}} = 8 \times 10^9 \text{ K km s}^{-1} \text{ pc}^2$, or $4 \times 10^{10} M_{\odot}$ of molecular gas. These are ~ 20 times greater than the CO luminosity and molecular mass of the Milky Way interior to the Solar circle (Solomon & Rivolo 1989). Previous CO surveys of spiral galaxies show there are many isolated, non-interacting spirals with CO luminosities 2 – 5 times higher than the Milky Way. Examples include NGC 6946, NGC 7479, and NGC 1530 (cf. Solomon & Sage 1988). A particularly gas rich, isolated galaxy with normal far IR properties is NGC 3147. Its CO luminosity and molecular mass are 15 times larger than the Milky Way’s and close to the average for these ultraluminous IR galaxies. High molecular masses appears, however, to be more common in interacting galaxies than in normal galaxies. In a group of 29 interacting galaxies with separations $< 5 D_{25}$ and some morphological disturbances, Solomon & Sage (1988) found 15 had molecular masses greater than $5 \times 10^9 M_{\odot}$. Below (section 5) we derive the molecular mass of ultraluminous galaxies by several methods, including estimates of the dynamical mass and of the H_2 mass for optically thin CO emission. We conclude the standard Milky Way $M(H_2)/L'_{\text{CO}}$ ratio overestimates the H_2 masses of these galaxies by a factor of three.

3.2. Infrared Luminosities and Dust Temperatures

From the fluxes in the IRAS Faint Source Catalog we calculated FIR luminosities (**Table 2**).

$$L_{\text{FIR}} = 3.94 \times 10^5 (2.58 S_{60} + S_{100}) r(S_{60}/S_{100}) D_L^2, \quad (4)$$

with L_{FIR} in L_{\odot} , S in Jy, and D_L in Mpc. The color correction, r , is a function of the $60 - 100 \mu\text{m}$ flux ratio and the assumed dust emissivity (Lonsdale et al. 1985). This is a multiplicative factor between 1.5 and 2.1 that allows the FIR luminosity to be derived from the 60 and $100 \mu\text{m}$ fluxes.

Note, we use far IR luminosity, L_{FIR} rather than IR luminosity, L_{IR} , which includes the $25 \mu\text{m}$ flux (Sanders et al. 1991). For the faintest galaxies in the sample the $25 \mu\text{m}$ flux has a large uncertainty and in any case contributes only about 20% to the total IR luminosity except for four warm objects with $25/60 \mu\text{m}$ ratios > 0.2 where L_{IR} is about 50% higher than L_{FIR} . In terms of IR luminosity the number of sources in the sample with $L_{\text{IR}} > 1 \times 10^{12} L_{\odot}$ remains at 25; there are another 7 with $L_{\text{IR}} > 0.8 \times 10^{12} L_{\odot}$.

The dust temperature derived from the far IR colors depends on the assumed emissivity for optically thin dust but is independent of emissivity for an optically thick source. While the dust in normal galaxies, including the Milky Way, is transparent in the far IR, there is strong evidence (next section and Condon et al. 1991) the dust in ultraluminous galaxies is opaque, even at 60 and $100 \mu\text{m}$. We used, therefore, a black body emissivity index, $n = 0$,

to calculate dust temperatures and color corrections. This gives higher dust temperatures than the optically thin approximation. The observed dust temperatures were also multiplied by $(1 + z)$ to obtain rest frame temperatures.

Figure 3 is a diagram of FIR luminosity vs. CO luminosity for the galaxies in our sample. For comparison, some well-known galaxies and the trend for normal and weakly interacting spirals (Solomon & Sage 1988) are also shown. Ultraluminous galaxies have a systematically higher infrared to CO luminosity ratio. In the following section we develop a model which explains the high ratio and shows that there is a clear upper limit to $L_{\text{FIR}}/L_{\text{CO}}$. The model also leads to a re-interpretation of the molecular mass determination for ultraluminous galaxies.

4. BLACK BODY MODEL

We argued previously (DSR) that for ultraluminous galaxies, the tight correlation of CO line intensity and $100\mu\text{m}$ flux strongly indicates the dust is optically thick at $100\mu\text{m}$. The essential steps in that argument were:

a) Small sizes of CO regions imply black bodies in the FIR. Interferometers show the molecular gas in ultraluminous galaxies is in small central regions. Examples are Arp 220, with a CO and HCN core radius of 320 pc (Scoville et al. 1991; Okumura et al. 1991; Radford et al. 1991b); Mrk 231, with a CO source radius 0.7 kpc (Bryant & Scoville 1996); and 17208 – 0014, with a CO radius < 1.2 kpc (Planesas, Mirabel, & Sanders 1991). The small CO sizes and the H_2 masses estimated from the CO luminosities yield column densities $n(\text{H}_2) \geq 10^{24} \text{ cm}^{-2}$. For a Galactic gas-to-dust mass ratio of 100 – 200, the standard relation for far IR dust opacity (e.g., Hildebrand 1983) then yields $\tau_{\text{dust}} > 1$ at $100\mu\text{m}$, so the far IR source is optically thick.

b) Tight correlation of I_{CO} with $100\mu\text{m}$ flux implies black body radiation. For the ultraluminous galaxies, CO integrated line intensity, I_{CO} , is tightly correlated with $100\mu\text{m}$ flux density (**Fig. 4**). The scatter in this correlation is about a factor of two. As we showed earlier (DSR), this flux-flux correlation can be understood if both the CO and the dust are optically thick. Not only does CO line intensity vary linearly with $100\mu\text{m}$ flux density, but the observed constant of proportionality agrees with the black body model. To demonstrate this, the argument in Downes, Solomon, & Radford (1993), that was given in terms of the monochromatic $100\mu\text{m}$ luminosity, L_{100} , will now be reformulated in terms of the total far IR luminosity L_{FIR} . In our earlier presentation of this argument, we assumed the CO linewidth ΔV was the same on all lines of sight; in this version, we allow for a velocity filling factor f_V .

Assume the CO traces a huge cloud of area filling factor unity and the dust is opaque for $\lambda \leq 100 \mu\text{m}$. The source may be a disk, a torus, a bar, or have an irregular shape. For illustration, we derive the luminosity ratio for a sphere, but as long as the CO and far IR sources cover the same area, the FIR/CO luminosity ratio is independent of source shape. For an optically thick sphere of temperature T_d at its outer radius R ,

$$L_{\text{FIR}} = 4\pi R^2 \sigma T_d^4 \quad , \quad (5)$$

where σ is the Stephan-Boltzmann constant. Similarly, the CO(1–0) luminosity

$$L_{\text{CO}} = 4\pi^2 R^2 \frac{2k}{\lambda^2} \int T_b d\nu \quad , \quad (6)$$

where T_b is the intrinsic brightness temperature, ν is frequency, and L_{CO} is in the same units as L_{FIR} (e.g., Watts or L_\odot). We assume that regardless of how the gas is clumped in volume, the region has an area filling factor of unity. If $T_b = T_d$,

$$\frac{L_{\text{FIR}}}{L_{\text{CO}}} = \frac{\sigma T_d^3 c^3}{2\pi k \nu_{\text{CO}}^3 f_V \Delta V} \quad , \quad (7)$$

where ν_{CO} is the CO(1–0) rest frequency and ΔV is the linewidth. For typical values,

$$\frac{L_{\text{FIR}}}{L_{\text{CO}}} = 4.8 \times 10^6 \left(\frac{T_d}{50K} \right)^3 \left(\frac{300}{f_V \Delta V} \right) \quad . \quad (8)$$

$$\frac{L_{\text{FIR}}}{L_{\text{CO}}} = 4.8 \times 10^6 \left(\frac{L_{\text{FIR}}}{10^{12} L_\odot} \right)^{3/4} \left(\frac{300 \text{ pc}}{R} \right)^{3/2} \left(\frac{300}{f_V \Delta V} \right) \quad . \quad (9)$$

With the CO luminosity in $\text{K km s}^{-1} \text{ pc}^2$,

$$L'_{\text{CO}} \equiv \pi R^2 T_b f_V \Delta V \quad , \quad (10)$$

the ratio becomes

$$\frac{L_{\text{FIR}}}{L'_{\text{CO}}} = \frac{4\sigma T_d^4}{f_V \Delta V T_b} \quad . \quad (11)$$

If $T_b = T_d$, then for typical values,

$$\frac{L_{\text{FIR}}}{L'_{\text{CO}}} = 224 \left(\frac{T_d}{50K} \right)^3 \left(\frac{300}{f_V \Delta V} \right) \quad , \quad (12)$$

where the $L_{\text{FIR}}/L'_{\text{CO}}$ ratio now has units of $L_\odot(\text{K km s}^{-1} \text{ pc}^2)^{-1}$.

Figure 5 shows this predicted ratio vs. dust temperature, for a typical $f_V \Delta V = 300 \text{ km s}^{-1}$, together with the observed ratios for ultraluminous galaxies in our sample. The median $L_{\text{FIR}}/L'_{\text{CO}} = 160 L_\odot/\text{K km s}^{-1} \text{ pc}^2$. This is within a factor of three

of the black body limit for temperatures 40 – 80 K. Galaxies with $L_{\text{FIR}} > 10^{12} \text{ L}_{\odot}$ are closer to the black body limit than the somewhat less luminous galaxies in our sample.

Normal spirals have $L_{\text{FIR}}/L'_{\text{CO}}$ ratios 10 to 30 times lower than the black body limit in **Fig. 5**. In normal spirals, the gas and dust extend over several kpc, so the column density is lower and the dust is transparent to its own radiation in the far IR. The black body limit applies if the same amount of matter is confined to a smaller volume, making the dust opaque and allowing *all* the dust to equilibrate with the radiation field. Ultraluminous galaxies indeed have $L_{\text{FIR}}/L'_{\text{CO}}$ ratios close to the black body limit, showing their far IR dust radiation is opaque at $\lambda \leq 100 \mu\text{m}$. The absence of strong near-mid IR ($25 \mu\text{m}$) peaks in 90% of our sample galaxies shows opaque dust blocks our view into warmer components where the spectrum peaks in the near IR, so we see only an enormous, $\sim 300 \text{ pc}$ photosphere at $\sim 60 \text{ K}$.

In reality, ultraluminous galaxies may differ from the black body model in the following respects:

a) CO brightness temperature \neq dust temperature. At the mean H_2 density in the central regions of ultraluminous galaxies (typically $\sim 10^3 - 10^4 \text{ cm}^{-3}$), the gas and dust are probably not coupled, so the gas kinetic temperature may be only about half the dust temperature. At that density, however, the *brightness* temperature of the CO(1–0) line will be close to the *gas* kinetic temperature. Although we took $T_b = T_d$ in our example, the argument is the same if the CO brightness temperature is half the dust temperature; the predicted $L_{\text{FIR}}/L'_{\text{CO}}$ is twice as large, that is, even higher than the observed values (**Fig. 5**).

b) CO size larger than far IR size. The gas probably occupies a larger volume than the opaque dust, which may be concentrated toward H II regions. If so, the radius in eq.(5) will be larger than that in eq. (4), lowering the predicted FIR/CO luminosity ratio toward the observed data (**Fig. 5**). Hence, a larger CO size compensates for a lower CO temperature, so the simple black body model may give the right ratio after all.

c) Area filling factors. We assumed area filling factors of unity, but real sources have windows through the opaque dust that allow us to see near IR radiation and, in some sources, optical lines (redshifts of these objects are measured from optical lines, some of which, however, may come from gas outside of the opaque nuclear regions). Provided the area filling factors are about the same in the far IR and in CO, the black body argument will be the same, and the predicted far IR to CO ratio will be as in the above equations.

5. CO SIZE AND MOLECULAR MASS

5.1. Radii Predicted by the Black Body Model

The black body equation (4) sets a lower limit to the far IR source size. In a more complex model with several optically thick, massive sources, the true radius would be larger, but the radiating surface area would remain the same. For some ultraluminous galaxies, the minimum radius is about the same size as the observed nonthermal radio source (Condon et al. 1991). This far IR black body radius (R_{bb} in **Table 3**) may also be compared to the minimum CO radius derived from eq. (9) with the assumptions that the dust and CO brightness temperatures are the same and the velocity filling factor f_V is unity.

$$R_{\text{CO}}(\text{min}) = L'_{\text{CO}} / (\pi T_{\text{bb}} \Delta V)^{0.5} \quad . \quad (13)$$

This is the minimum radius a CO source would have if its brightness temperature does not exceed the black body dust temperature. For the sources in our sample, the minimum CO radius (**Table 3**) is typically twice as large as the far IR black body radius, although sometimes the two agree. If these conditions are not fulfilled (e.g., a core-halo source), then the CO core radius scales as:

$$R_{\text{CO}}(\text{core}) = R_{\text{CO}}(\text{min}) \left(\frac{1}{f_V} \right)^{0.5} \left(\frac{L'_{\text{core}}}{L'} \right)^{0.5} \left(\frac{T_{\text{bb}}}{T_b} \right)^{0.5} \quad (14)$$

The minimum observed linewidths (**Table 1**) are $\sim 150 \text{ km s}^{-1}$, presumably from the face-on galaxies, while the larger observed linewidths suggest a true rotation velocity $V \sim 300 \text{ km s}^{-1}$. The velocity filling factor f_V would thus be $150/300 = 0.5$ for edge-on galaxies, and 1.0 for face-on galaxies. Interferometer observations of a few ultraluminous galaxies (e.g., Scoville et al. 1991) suggest $(L'_{\text{core}}/L') = 0.5$, and $T_{\text{bb}}/T_b = 2$. Hence on average, the true CO core radii may be $\sqrt{2}$ times larger than the minimum CO core radii listed in **Table 3**.

5.2. Dynamical Mass as an Upper Limit on Gas Mass

We calculated dynamical masses for the central regions of the ultraluminous galaxies by using the black body dust temperature derived from the $60/100 \mu\text{m}$ flux ratio to obtain a radius for the CO emitting region with eq.(12). We assume the characteristic velocity V in this region is determined by gravity, so the enclosed dynamical mass is $R_{\text{CO}} V^2 / G$, or

$$M_{\text{dyn}} = \left(\frac{L_{\text{CO}}}{\pi T_b f_V \Delta V} \right)^{0.5} \frac{V^2}{G} \quad . \quad (15)$$

For a velocity filling factor $f_V = 1$, the CO radius is a minimum radius, so a dynamical mass estimated this way is also a minimum value. As above, T_b is the CO intrinsic brightness

temperature (assumed here to be the black body dust temperature), ΔV is the observed CO linewidth (**Table 1**), and V is the true velocity in the region.

In our sample, galaxy inclinations are unknown, so we estimated the true velocity V statistically. The histogram of CO linewidths for the sample (**Fig. 6**) has a median of 300 km s^{-1} . We therefore assumed all the galaxies in our sample had a minimum internal velocity of 300 km s^{-1} , and that those with smaller observed linewidths were inclined to our line of sight. The face-on galaxies are those with the minimum observed linewidths of $\sim 150 \text{ km s}^{-1}$. To calculate minimum dynamical masses listed in **Table 3**, we thus took the minimum CO core radii, with $f_V = 1$ in eq.(9), and we took $V = \max(300 \text{ km s}^{-1}, \Delta V)$. If the motions are primarily radial, then $V = 3^{0.5} \Delta V$.

We also list in **Table 3** the equivalent total H_2 density, n_{tot} , a maximum to the true volume-averaged H_2 density, derived from the dynamical masses and the minimum CO radii. To calculate the minimum CO radii, we assumed thermalization, with the CO(1–0) brightness temperature equal to the gas kinetic temperature. At a kinetic temperature of 60 K, this would occur for H_2 densities $> 1500 \text{ cm}^{-3}$. Even if the CO emitting gas were to evenly fill the volume inside R_{CO} as an intercloud medium, the CO rotational levels would be thermalized in about half of the sources.

Since the gas mass, $M(\text{H}_2)$, cannot exceed the dynamical mass, the average ratio $M_{\text{dyn}}/L'_{\text{CO}} = 1.4$ (**Table 3**) suggests that α , the H_2 -mass-to-CO-luminosity ratio, may be at least three times lower than in Galactic molecular clouds. This is consistent with the black body model. For gravitationally bound clouds, this ratio is $\alpha = 2.1 \cdot n^{0.5}/T_b$ (e.g., Radford, et al. 1991a); CO thermalization requires that $n(\text{H}_2) = 2000 \text{ cm}^{-3}$ to obtain $T_b = 60 \text{ K}$, yielding $\alpha \approx 1.6 \text{ M}_\odot/\text{K km s}^{-1} \text{ pc}^2$.

The dynamical mass listed in **Table 3** is the minimum dynamical mass of a core source that has *all* the observed CO luminosity, L'_{CO} , a CO brightness temperature $T_b(\text{CO})$ equal to the far IR black body temperature T_{bb} , and a velocity filling factor $f_V = 1$. If these assumptions are not fulfilled (e.g., a core-halo source), then dynamical mass scales linearly with $R_{\text{CO}}(\text{core})$ as in eq.(13). Hence to get the true dynamical mass in the CO core region, the values of $M_{\text{dyn}}(\text{min})$ in **Table 3** should be multiplied by

$$\frac{M_{\text{dyn}}(\text{core})}{M_{\text{dyn}}(\text{min})} = \left(\frac{1}{f_V}\right)^{0.5} \left(\frac{L'_{\text{core}}}{L'}\right)^{0.5} \left(\frac{T_{\text{bb}}}{T_b(\text{CO})}\right)^{0.5}. \quad (16)$$

Similarly, the ratio $M_{\text{dyn}}(\text{min})/L'_{\text{CO}}$ listed in **Table 3** can be scaled by the same factor to get the true ratio of core dynamical mass to total CO luminosity:

$$\frac{M_{\text{dyn}}(\text{core})}{L'_{\text{CO}}} = \frac{M_{\text{dyn}}(\text{min})}{L'_{\text{CO}}} \left(\frac{1}{f_V}\right)^{0.5} \left(\frac{L'_{\text{core}}}{L'}\right)^{0.5} \left(\frac{T_{\text{bb}}}{T_b(\text{CO})}\right)^{0.5}. \quad (17)$$

For the values suggested above, namely, $f_V = 0.5$, $(L'_{\text{core}}/L') = 0.5$, and $T_{\text{bb}}/T_b(\text{CO}) = 2$,

the true dynamical mass and the ratio M_{dyn}/L' would both be $\sqrt{2}$ times higher than the values in **Table 3**.

A check on the dynamical masses derived here can be provided by the fits to the 2.3 μm bandhead absorption originating in stellar atmospheres to estimate the velocity dispersion of the nuclear bulge stars. In a 1.5'' square aperture centered on NGC 6240S, Lester & Gaffney (1994) find $\sigma = 350 \text{ km s}^{-1}$, and estimate $M(< 260 \text{ pc}) = 2 R \sigma^2/G = 1.9 \times 10^{10} M_{\odot}$. This agrees reasonably well with our measurement (**Table 3**), of $\Delta V = 370 \text{ km s}^{-1}$, and $M(< 340 \text{ pc}) = R \Delta V^2/G = 1.1 \times 10^{10} M_{\odot}$. A similar estimate has been made for Arp 220 by Shier, Rieke, & Rieke (1994), yielding $M(< 350 \text{ pc}) = 1.8 \times 10^9 M_{\odot}$, which is ten times lower than our estimate of the dynamical mass (**Table 3**). This is mainly due to the low velocity dispersion of only 125 km s^{-1} deduced by Shier et al., whereas we took the observed Arp 220 CO linewidth of 480 km s^{-1} . The large CO linewidth is also present in our millimeter spectra of HCN and CS. We suspect that the 2 μm CO bandhead data from Arp 220 may be affected by the heavy extinction to the western near IR peak, and may not refer to the same volume as the millimeter line data.

5.3. Lower Limit to H_2 Mass: Optically Thin CO

Since CO is always optically thick in Milky Way GMC's and spiral galaxies, we can get a useful lower limit to the H_2 mass by assuming the CO(1–0) line has an optical depth $\tau \leq 1.0$. The minimum H_2 gas mass is then

$$M_{\text{thin}} = 6.9 \times 10^{-3} M_{\odot} L'_{\text{CO}} T_b \quad (18)$$

for L'_{CO} in $\text{K km s}^{-1} \text{ pc}^2$ and T_b in K. We assume the rotational levels are thermalized and the CO/ H_2 abundance ratio is 1.0×10^{-4} . The black body model for T_b and the observed line luminosities yield an optically thin molecular mass given in **Table 4**. They are typically $2 - 5 \times 10^9 M_{\odot}$, or about one-third the dynamical mass. Even if the emission is optically thin a large fraction of the dynamical mass is H_2 with $M_{\text{thin}} = 0.34 \pm 0.12 M_{\text{dyn}}$. Evidence from CO excitation points to optical depths $\tau > 1.0$ (Radford, et al. 1991a) indicating that a mass based on the optically thin approximation is good lower limit. In this model, if the CO optical depth is only ~ 3 , then molecular gas alone would account for most of the dynamical mass. While the assumption of thermalized rotational levels may increase the thin mass estimate by a factor of 2 due to an overestimate of the partition function, this will be more than compensated for by the realistic optical depth. The *minimum* (optically thin) molecular mass would be lower only if the metallicity were significantly greater than Solar and the CO/ H_2 abundance ratio much greater than in Milky Way GMC's.

5.4. Dust Mass from 100 μm Emission

An alternative method of estimating the mass of molecular gas which is independent of spectral line observations is to use the far infrared emission and assume the dust is optically thin. This is, of course, inconsistent with the black body model of optically thick dust but it provides an alternative measure of mass. To calculate the dust mass we assume the dust is thin, its emissivity varies as $\lambda^{-1.5}$, and its far IR emission coefficient is that given by Hildebrand (1983). This should be regarded as a rough estimate since IR emissivity of dust in molecular clouds is not well calibrated. The dust temperature determined from the 60/100 μm ratio is typically 40 – 50 K, and the mass is estimated from the 100 μm flux. Since this measures only warm dust radiating at 100 μm , it is strictly a lower limit to the total dust mass. Near the center of a galaxy, however, most of the dust will indeed be warm. If we further assume the gas-to-dust mass ratio is 100, the total molecular mass can be calculated (column 4 of **Table 4**). The average gas mass estimated from the warm dust emission is very close to the dynamical mass, with $100 M_{\text{dust}} = 1.1 \pm 0.5 M_{\text{dyn}}$

5.5. Modified H_2 mass-to-CO luminosity Relation

For a galaxy containing virialized molecular clouds, the H_2 mass-to-CO luminosity relation can be expressed as

$$M'(\text{H}_2) = \alpha L'_{\text{CO}}. \quad (19)$$

Use of the Milky Way H_2 mass-to-CO luminosity ratio, $\alpha = 4.6 \text{ M}_\odot/\text{K km s}^{-1} \text{ pc}^2$, clearly overestimates the H_2 mass in ultraluminous galaxies (**Table 2**). We previously (DSR) related the CO luminosity to the dynamical mass as well as the H_2 mass. This model may explain why the true gas masses are lower than the masses derived with the Milky Way ratio. The key point is that unlike Galactic clouds or gas distributed in the disks of galaxies, the CO in the centers of ultraluminous galaxies may *not* come from virialized clouds, but from a filled intercloud medium, so *the linewidth is determined by the total dynamical mass in the region (gas and stars)*, that is, $\Delta V^2 = G M_{\text{dyn}}/R$. The CO line emission may trace a medium bound by the total potential of the galactic center, containing a mass M_{dyn} consisting of stars, dense clumps, and an interclump medium containing the CO emitting gas with mass $M(\text{H}_2)$.

Defining $f \equiv M(\text{gas})/M_{\text{dyn}}$, we showed the usual CO to H_2 mass relation becomes

$$M_{\text{dyn}}/L'_{\text{CO}} = f^{-1/2} \alpha = f^{-1/2} 2.6 (\bar{n})^{1/2} T_b^{-1}, \quad (20)$$

$$M(\text{H}_2)/L'_{\text{CO}} = f^{1/2} \alpha = f^{1/2} 2.6 (\bar{n})^{1/2} T_b^{-1}, \quad (21)$$

and

$$M_{\text{dyn}} M(\text{H}_2) = (\alpha L'_{\text{CO}})^2 , \quad (22)$$

where \bar{n} is the H_2 density averaged over the whole volume. We argued in our earlier paper that the quantity $\alpha L'_{\text{CO}}$ measures the geometric mean of total mass and gas mass. It underestimates total mass and overestimates gas mass. Hence if the CO emission in ultraluminous galaxies comes from regions not confined by self gravity, but instead from an intercloud medium bound by the potential of the galaxy, or from molecular gas in pressure, rather than gravitational, equilibrium, then the usual relation $M(\text{H}_2)/L'_{\text{CO}} = \alpha$ must be changed to eq.(20).

5.6. Summary of Revised Mass Estimates

For the compact central regions, the dynamical mass is the best estimator of the molecular mass. The dynamical masses listed in **Table 4** are those for the black-body model; the actual dynamical mass is given by eq.(15). We have argued here that the black-body model is a good approximation for ultraluminous galaxies since it comes close to predicting the ratio of far IR to CO luminosity. The CO luminosity to molecular mass conversion factor for ultraluminous galaxies must be $\leq M_{\text{dyn}}/L'_{\text{CO}} \sim 1.4$. is given in **Table 3**). Our estimates of the gas mass from optically thin CO(1-0) (Column 3 of **Table 4**) and from optically thin dust (Column 4 of **Table 4**) indicate that a large fraction of the dynamical mass is molecular gas (i.e., f approaches 1 in equations 19 and 20). If the dynamical mass is dominated by the gas mass and the core size is close to that of the black-body model then

$$M(\text{H}_2) = 1.0 \times 10^{10} M_{\odot} , \quad (23)$$

with a dispersion of only $0.3 \times 10^{10} M_{\odot}$. This is about three times lower than previous estimates of the gas mass which have utilized the Milky Way $M(\text{H}_2)/L'_{\text{CO}}$ ratio. Even if the velocity filling factor is 0.5 and the excitation temperature half that of the dust the dynamical mass is only increased by a factor of 2. More accurate determinations of the dynamical mass will come from interferometer measurements of the CO radii for the nearer galaxies in the survey.

The standard $M'(\text{H}_2)/L'_{\text{CO}} = 4.6 M_{\odot}/\text{K km s}^{-1} \text{ pc}^2$ (Column 2 of **Table 2**), appropriate for the molecular gas in a more typical galactic environment outside the central core, is an overestimate for ultraluminous galaxies.

6. PAIR SEPARATION AND $L_{\text{FIR}}/L_{\text{CO}}$ OF ULTRALUMINOUS GALAXIES

The prevalence of close interactions among IR bright galaxies was noted soon after the first IRAS galaxy catalog became available (Lonsdale, Persson, & Matthews 1984; Soifer et al. 1984). In **Fig. 7** we present R-band CCD images of 12 sample galaxies between RA 10h to 23h (Sanders & Kim, private communication); they show a wide variation in morphology and pair separation. Some appear distinctly single, with only slightly distorted disks, e.g., 1609–0139, while others are prominent, closely interacting galaxies with two disks and two nuclei, e.g., 10190+1322 or 15030+4835. One of the most luminous and most distant objects in our sample, 14070+0525, appears to be an isolated galaxy, although very faint tails would be invisible on this image. **Table 5** summarizes the data on pair separation for the sample, from the literature and from **Fig. 7**. The measured separations range from 0.3 to 14 kpc with an average of 6 kpc. Near IR images of some close ultraluminous galaxies such as Arp 220 and Mrk 231 show that galaxies apparently single in optical images may have double nuclei with small separations, indicating a nearly completed merger (Graham et al. 1990; Majewski et al. 1993; Armus et al. 1994). Conversely some galaxies which appear double in optical images clearly have only one nucleus in K band images (Murphy et al. 1996). Given the large amount of dust in these objects, however, even the near IR images may be heavily affected by extinction, and suspected double nuclei may actually be bright objects outside of the heavily obscured CO-emitting zone.

On the basis of R band images of ten nearby ultraluminous galaxies, Sanders et al. (1988a) argued that all ultraluminous galaxies are strongly interacting, as shown by tidal tails, rings or double nuclei with separations < 5 kpc, and that the fraction of close doubles increases with IR luminosity. From optical morphology and spectra, they suggested ultraluminous galaxies represent the initial dust enshrouded stage in the formation of quasars. In their model, most of the luminosity comes from an AGN rather than star formation. Because very few of the ultraluminous galaxies found by IRAS have true quasar or Seyfert 1 spectra, Sanders et al. argued the AGN was completely hidden by dust and the transition phase to a dust-free AGN is represented by the “warm” ultraluminous galaxies with $S_{25}/S_{60} > 0.2$ (Sanders et al. 1988b). Only five of the objects in our sample have $S_{25}/S_{60} > 0.2$ and four of these overlap with Sanders et al.’s sample. However, the object with the highest $L_{\text{FIR}}/L'_{\text{CO}}$, 08572+3915, is a warm galaxy but is definitely not a completed merger since its separation is 5.5 kpc (Sanders 1992).

There are no significant correlations of pair separation (Table 5) with CO luminosity or more importantly the ratio of far IR to CO luminosity, $L_{\text{FIR}}/L'_{\text{CO}}$. The apparent stage of the interaction appears to have little effect on the efficiency of star formation or the fueling of the putative black hole. Extremely luminous infrared galaxies include completed mergers

and interacting pairs with separations of approximately 10kpc. Two of the more distant and more luminous objects in our sample, 16334+4630 and 15030+4835, with very cool far IR colors, have large pair separations, 11 and 12 kpc (**Fig. 7**) respectively. Both have $L_{\text{FIR}} \approx 2 \times 10^{12} L_{\odot}$, similar to Mrk 231 or the quasar Mrk 1014. If an evolutionary sequence is present in ultraluminous galaxies it is not apparent from the CO or IR data combined with the optical morphology.

7. DISCUSSION

7.1. Dense Molecular Gas

In addition to a high IR/CO luminosity ratio, the molecular gas in the centers of ultraluminous galaxies exhibits other differences from GMC's in the Milky Way and normal spiral galaxies. Most important is the extremely high HCN luminosity. HCN emission traces H₂ at a much higher density, $\sim 10^5$ cm⁻³, than CO (~ 500 cm⁻³). As we have shown previously, the HCN luminosities of the ultraluminous galaxies Mrk 231, Arp 220, and NGC 6240 are greater than the CO luminosity of the Milky Way (Solomon, Downes, & Radford 1992a). The ratio of HCN to CO luminosity is 1/4 to 1/7 for ultraluminous galaxies, but only 1/30 or less in the disks of normal spiral galaxies. This implies that a large fraction of the molecular gas in ultraluminous galaxies, perhaps 50%, is in very dense regions similar to star forming cloud cores in Orion or W51, rather than in the envelopes of giant molecular clouds, as is the case in the disks of normal spiral galaxies.

If galactic HCN luminosity is taken as a dense gas indicator and far infrared luminosity as a high mass star formation indicator, then the star formation rate per mass of *dense* gas is the same for normal spirals and IR luminous interacting galaxies. There is sufficient dense gas in ultraluminous galaxies to account for their luminosity by star formation. In our model, the CO emission from ultraluminous galaxies originates from an intercloud medium essentially filling the volume; the emission from HCN and CS is from the dense “clouds” embedded inside the molecular region. The entire ISM is a scaled up version of a normal galactic disk. This environment is an ideal stellar nursery for prodigious star formation leading to ultraluminous galaxies.

7.2. Summary of CO Observations and H₂ Mass

Of the 37 galaxies in the sample, 32 have a far infrared luminosity greater than $6.5 \times 10^{11} L_{\odot}$ and total IR luminosities greater than $8 \times 10^{11} L_{\odot}$. We refer to these as ultraluminous IR galaxies. They share several properties in common:

1. All but one of the ultraluminous galaxies have a high CO(1-0) luminosity, with values of $\log (L'_{\text{CO}}/\text{K km s}^{-1} \text{ pc}^2) = 9.92 \pm 0.12$. The extremely small dispersion of only 30 % is half that of the far infrared luminosity. The parameter with the narrowest range (best defined) is not IR luminosity but CO luminosity, even though the selection was based on IR luminosity.

2. We have demonstrated that for ultraluminous galaxies in which the central few hundred parsecs is dominated by a molecular core, the CO luminosity and the ratio of FIR to CO luminosity can be explained as a consequence of thermal emission from optically thick dust and CO in a central sphere, torus (ring) or disk. The ambient densities are a factor of 100 higher than in a galactic disk, making even the intercloud medium molecular throughout. The median value of $L_{\text{FIR}}/L'_{\text{CO}} = 160 \text{ L}_\odot/\text{K km s}^{-1} \text{ pc}^2$, within a factor of 2 of the black body limit for the observed far IR temperatures.
3. From the observed linewidths, we estimate the dynamical mass within the minimum CO radius ($\sim 400 \text{ pc}$). This provides an upper limit on the mass of molecular gas. For a velocity filling factor of 1.0, the dynamical mass is $1.0 \pm 0.3 \times 10^{10} \text{ M}_\odot$. A more likely velocity filling factor of 0.5 raises the upper limit to the mass by $2^{0.5}$.
4. We assume the CO is optically thin in the (1–0) line to estimate the gas mass from the observed CO luminosity. This provides a lower limit on the mass of molecular gas of typically $2 - 5 \times 10^9 \text{ M}_\odot$, with $M_{\text{thin}} = 0.34 \pm 0.12 M_{\text{dyn}}$ or about one-third the dynamical mass.
5. We assume the dust is optically thin at $100 \mu\text{m}$ to estimate the minimum mass of interstellar material. This provides another, independent measure of the mass of molecular gas. The average gas mass estimated from the dust continuum emission assuming a dust to gas ratio of 100 is very close to the dynamical mass, $100 M_{\text{dust}} = 1.1 \pm 0.5 M_{\text{dyn}}$.
6. The standard Milky Way ratio, $M'(\text{H}_2)/L'_{\text{CO}} = 4.6 \text{ M}_\odot(\text{K km s}^{-1} \text{ pc}^2)^{-1}$, yields a mass $M'(\text{H}_2) = 3.7 M_{\text{dyn}}$, which is clearly an overestimate. We show that in the extreme environment near the center of an ultraluminous galaxy, where the CO emission originates from an intercloud medium which essentially fills a volume rather than from clouds bound by self gravity, the CO luminosity traces the geometric mean of the molecular mass and the total dynamical mass. The true total molecular mass must be between the optically thin CO estimate and the dynamical mass. The agreement between the total gas mass estimated from the dust emission and the dynamical mass suggests a number closer to the dynamical mass. Dynamical mass estimates with sizes determined from interferometer measurements are required to obtain better estimates of the molecular mass in ultraluminous galaxies.

7.3. The Effect of Close Interactions on the Molecular ISM

Molecular clouds are in virial equilibrium, not pressure equilibrium, (eg. Solomon et al., 1987) maintained by a balance between self gravity and turbulence driven primarily by star formation. The external pressure from the ambient ISM or intercloud medium is significantly less than the internal effective pressure characterized by supersonic velocities. The star formation is self regulating and GMC's in galactic disks have modest star formation rates per solar mass (Mooney and Solomon, 1988).

The uniformly high CO luminosities found here for all ultraluminous galaxies, combined with the evidence of very large quantities of even denser molecular gas, show that the molecular gas required for an extreme starburst is always present when a galaxy has ultrahigh infrared luminosity. Does this imply that a merger or close interaction is the ideal site for the transformation of diffuse gas into molecular clouds or the stimulation of high mass star formation by cloud collisions (eg. Scoville, Sanders & Clemens, 1986)? Both seem highly unlikely given the typical interaction velocity of 200 or 300 km/s, more than an order of magnitude greater than the escape velocity of material in even the most massive GMC's, and more than sufficient to completely ionize and destroy any trace of molecules in a direct collision between clouds. The molecular gas in luminous mergers must be from **preexisting** molecular clouds. Unlike diffuse gas, the mean free path for molecular clouds is sufficiently long (~ 2 kpc) that a merger, unless it is completely edge on, will result in few direct collisions. Molecular clouds can therefore survive a close interaction or merger, although they will be changed by the new environment.

Two mechanisms have been proposed for triggering an intense burst of star formation in preexisting molecular clouds during a close interaction or merger. During a direct collision the HI clouds will collide, forming a hot ionized high pressure remnant gas (Jog and Solomon, 1992). The overpressure due to this hot gas causes a radiative shock compression of the outer layers of GMC's in the overlapping wedge region. The outer layers become gravitationally unstable, leading to a burst of star formation in the initially stable GMC's. This scenario probably applies to luminous ($\sim 10^{11}L_{\odot}$) IR galaxies with prominent extranuclear starbursts such as Arp 299, but is not strong enough to produce ultraluminous galaxies. A more efficient mechanism for producing a central starburst in interacting galaxy pairs from preexisting clouds has been suggested by Jog and Das (1992). In this model, as a disk GMC tumbles into the central regions of a galaxy following an encounter, it undergoes radiative shock compression by the high pressure of the central molecular intercloud medium. When the growth time for the gravitational instabilities in the shocked outer shell of a cloud becomes smaller than the shock crossing time, the shell becomes unstable, resulting in a burst of star formation. The infall may be helped by the establishment of a nonaxisymmetric bar potential (eg. Norman , 1991). The luminosity

depends on the compressed mass fraction, cloud infall rate and efficiency of star formation; evolved mergers generate a luminosity comparable to that of ultraluminous IR galaxies.

Our analysis of CO emission from ultraluminous galaxies reduces the H₂ mass from previous estimates of $2-5 \times 10^{10} M_{\odot}$ to $0.4-1.0 \times 10^{10} M_{\odot}$, which is in the range found for molecular gas rich spiral galaxies. Thus a collision involving a molecular gas rich spiral could lead to an ultraluminous galaxy powered by central starbursts triggered by the compression of preexisting GMC's.

We thank Mr. Yu Gao, Stony Brook, for help with Table 5, and Fred Seward, Elizabeth Bohlen, and the Center for Astrophysics for the use of their measuring engine. We especially thank D. B. Sanders and D. C. Kim for letting us use their R band CCD images.

REFERENCES

Armus, L., Heckman, T.M., & Miley, G.K. 1987, AJ, 94, 831

Armus, L., Heckman, T.M., & Miley, G.K. 1990, ApJ, 364, 471

Armus, L., Surace, J.A., Soifer, B.T., Matthews, K., Graham, J.R., & Larkin, J.E. 1994, AJ, 108, 76

Barvainis, R., Alloin, D., & Antonucci, R. 1989, ApJ, 337, L69

Beichman, C.A., Neugebauer, G., Habing, H.J., Clegg, P.E., Chester, T.J. (eds.) 1988, IRAS Catalogs and Atlases Explanatory Supplement, (Washington, D.C.: U.S. Govt. Printing Office)

Bryant, P.M., & Scoville, N.Z. 1996, ApJ, 457, 692

Condon, J.J., Huang, Z.P., Yin, Q.F., & Thuan, T.X. 1991, ApJ, 378, 65

Downes, D., Solomon, P.M., & Radford, S.J.E. 1993, ApJ, 414, L13 (DSR).

Fisher, K.B., Huchra, J.P., Strauss, M.A., Davis, M., Yahil, A., & Schlegel, D. 1995, ApJS, 100, 69

Graham, J.R., Carico, D.P., Matthews, K., Neugebauer, G., Soifer, B.T., & Wilson, T.D. 1990, ApJ, 354, L5

Hildebrand, R.H. 1983, QJRAS, 24, 267

Infrared Astronomical Satellite (IRAS) Point Source Catalog, Version 2 1988, Joint IRAS Science Working Group, (Washington, D.C.: U.S. Govt. Printing Office)

Jog, C.J., & Solomon, P.M. 1992, ApJ, 387, 152

Jog, C.J., & Das, M. 1992, ApJ, 400, 476

Kollatschny, W., Dietrich, M., Borgeest, U., & Schramm, K.J. 1991, A&A, 249, 57

Lester, D.F., & Gaffney, N.I. 1994, ApJ, 431, L13

Lonsdale, C.J., Persson, S.E., & Matthews, K. 1984, ApJ, 287, 95

Lonsdale, C.J., Helou, G., Good, J.C., & Rice, W. 1985, in Cataloged Galaxies and Quasars Observed in the IRAS Survey, (Pasadena: JPL)

Majewski, S.R., Hereld, M., Koo, D.C., Illingworth, G.D., & Heckman, T.M. 1993, ApJ, 402, 76

Melnick, J. & Mirabel, I.F. 1990, A&A, 231, L19

Mihos, J.C., & Hernquist, L. 1994, ApJ, 431, L9

Mooney, T. & Solomon, P.M. 1988, *ApJ*, 334, L51

Moshir et al. 1992, IRAS Faint Source Survey Explanatory Supplement, Version 2, (Pasadena: JPL)

Murphy, T.W. Jr., Armus L., Matthews, K., Soifer, B.T., Mazzarella, J.M., & Shupe, D.L. 1996, *AJ*, 111, 1025

Norman, C. A. 1991, in *Massive Stars in Starbursts*, ed. C. Leitherer, N.R. Walborn, T.M. Heckman, & C.A. Norman, (Cambridge: Camb. Univ. Press) 271

Okumura, S.K., Kawabe, R., Ishiguro, M., Kasuga, T., Morita, K.I., & Ishizuki, S. 1991, in *Dynamics of Galaxies and Their Molecular Cloud Distributions*, ed. F. Combes & F. Casoli (Dordrecht: Kluwer), 425

Planesas, P., Mirabel, I.F., & Sanders, D.B. 1991, *ApJ*, 370, 172

Radford, S.J.E., Solomon, P.M., & Downes, D. 1991a, *ApJ*, 368, L15

Radford, S.J.E., et al. 1991b, in *Dynamics of Galaxies and Their Molecular Cloud Distributions*, ed. F. Combes & F. Casoli (Dordrecht: Kluwer), 303

Sanders, D.B. 1992, in *Relationships Between Active Galactic Nuclei and Starburst Galaxies*, ASP Conf. Ser. 31, ed. A.V. Filippenko, (San Francisco: ASP) 303

Sanders, D.B., Soifer, B.T., Elias, J.H., Madore, B.F., Matthews, K., Neugebauer, G., & Scoville, N.Z. 1988a, *ApJ*, 325, 74

Sanders, D.B., Soifer, B.T., Elias, J.H., Neugebauer, G., & Matthews, K. 1988b, *ApJ*, 328, L35

Sanders, D.B., Scoville, N.Z., & Soifer, B.T. 1991, *ApJ*, 370, 158

Sanders, D.B., et al., 1986, *ApJ*, 305, L45

Scoville, N.Z., Sanders, D.B., & Clemens, D.P., 1986, *ApJ*, 310, L77

Scoville, N.Z., Sargent, A.I., Sanders, D.B., & Soifer, B.T. 1991, *ApJ*, 366, L5

Shaya, E.J., Dowling, D.M., Currie, D.G., Faber, S.M., & Groth, E.J. 1994, *AJ*, 107, 1675

Shier, L.M., Rieke, M.J., & Rieke, G.H. 1994, *ApJ*, 433, L9

Soifer, B.T., et al. 1984, *ApJ*, 278, L71

Solomon, P.M., Downes, D., & Radford, S.J.E. 1992a, *ApJ*, 387, L55

Solomon, P.M., Radford, S.J.E., & Downes, D. 1990, *ApJ*, 348, L53

Solomon, P.M., Radford, S.J.E., & Downes, D. 1992, *Nature*, 356, 318

Solomon, P.M., & Rivolo, A.R. 1989, *ApJ*, 339, 919

Solomon, P.M., Rivolo, A.R., Barrett, J.W., & Yahil, A. 1987, ApJ, 319, 730

Solomon, P.M., & Sage, L.J. 1988, ApJ, 334, 613

Strauss, M.A., Huchra, J.P., Davis, M., Yahil, A., Fisher, K.B., & Tonry, J. 1992, ApJS, 83, 29

Wright, G.S., Joseph, R. D. & Meikle, W.P. 1984, Nature, **344** 417

Weinberg, S. 1972, *Gravitation and Cosmology* (New York: Wiley)

Table 1. DATA FROM THE IRAM 30 m TELESCOPE ON CO(1–0) IN ULTRALUMINOUS GALAXIES

Source name	Position R.A. 1950 (h m s)	Observed Dec. 1950 (° ' ")	Redshift cz (km s $^{-1}$)	Linewidth ΔV (km s $^{-1}$)	Intensity I_{CO} (K km s $^{-1}$)	CO/FIR $I_{CO}/S_{100\mu m}$ (K km s $^{-1}$ Jy $^{-1}$)
00057+4021	00 05 45.1	+40 21 14	13390	350	9.9	2.30
00188–0856	00 18 53.7	–08 56 07	38530	390	2.2	0.65
00262+4251	00 26 12.9	+42 51 40	29153	230	3.5	1.43
I Zw 1	00 50 57.8	+12 25 19	18330	410	7.0 ^{b)}	2.66
Mrk 1014	01 57 16.6	+00 09 07	48947	200	1.8	0.83
02483+4302	02 48 20.4	+43 02 56	15419	250	5.7	0.82
03158+4227	03 15 52.3	+42 27 36	40296	180	2.1	0.49
03521+0028	03 52 07.8	+00 28 20	45530	150	2.2	0.57
04232+1436	04 23 15.2	+14 36 53	23855	400	7.5	1.76
VII Zw 31	05 08 17.5	+79 36 40	16260	200	21.0	2.18
07598+6508	07 59 53.0	+65 08 21	44621 ^{a)}	337	2.8 ^{a)}	1.62
08030+5243	08 03 01.5	+52 43 45	25031	420	6.7	1.53
08572+3915	08 57 13.0	+39 15 39	17450	270	2.0	0.44
09320+6134	09 32 04.7	+61 34 37	11785	350	15.6	0.77
10035+4852	10 03 35.5	+48 52 25	19427	250	8.8	1.41
10190+1322	10 19 01.4	+13 22 04	22953	390	7.4	1.33
10495+4424	10 49 30.1	+44 24 46	27674	330	5.1	0.94
10565+2448	10 56 35.4	+24 48 43	12923	300	15.7	1.04
11506+1331	11 50 39.8	+13 31 05	38158	290	2.5	0.75
Mrk 231	12 54 05.0	+57 08 39	12650	230	22.0	0.73
13106–0922	13 10 37.3	–09 22 15	52290	200	1.7	0.70
Arp 193	13 18 17.0	+34 24 07	7000	410	36.0	1.43
Mrk 273	13 42 51.6	+56 08 14	11324	300	19.0	0.89
13442+2321	13 44 18.0	+23 21 14	42620	140	1.4	0.62
14070+0525	14 07 00.5	+05 25 41	79621	270	0.8	0.42

Table 1—Continued

Source name	Position R.A. 1950 (h m s)	Observed Dec. 1950 (° ' ")	Redshift <i>cz</i> (km s ⁻¹)	Linewidth ΔV (km s ⁻¹)	Intensity I_{CO} (K km s ⁻¹)	CO/FIR $I_{\text{CO}}/S_{100\mu\text{m}}$ (K km s ⁻¹ Jy ⁻¹)
15030+4835	15 03 01.3	+48 35 24	64900	270	1.5	1.03
Arp 220	15 32 46.9	+23 40 08	5450	480	109.0	0.97
16090–0139	16 09 04.9	–01 39 25	40044	300	3.7	0.76
16334+4630	16 33 24.3	+46 30 58	57250	320	1.5	0.69
NGC 6240	16 50 27.2	+02 28 58	7298	370	69.0	2.48
17208–0014	17 20 48.2	–00 14 17	12837	360	20.0	0.57
18368+3549	18 36 49.5	+35 49 36	34850	330	3.4	0.89
19297–0406	19 29 43.1	–04 06 24	25700	300	6.8	0.88
19458+0944	19 45 52.0	+09 44 30	29980	350	6.4	0.90
20087–0308	20 08 46.4	–03 08 52	31688	400	7.7	1.18
22542+0833	22 54 11.3	+08 33 22	49750	150	1.2	0.81
23365+3604	23 36 32.3	+36 04 34	19330	310	10.7	1.28
<i>median:</i>	—	—		300	—	0.9
<i>std. dev.:</i>	—	—		85	—	0.6

^{a)}Sanders et al. (1988b), I_{CO} corrected by us; ^{b)}Barvainis et al. (1989).

Errors: cz : ± 20 km s⁻¹; ΔV : ± 30 km s⁻¹; I_{CO} : $\pm 20\%$ for $I > 6$, $\pm 35\%$ for $2 < I < 6$. Linewidths are Gaussian fit values (FWHP), or else half the full width to zero intensity for non-gaussian lines (See **Figure 2** for spectra).

For point sources, $S/T_{\text{mb}} = 4.5$ Jy/K at the 30 m telescope at 3 mm.

Table 2. CO and far IR Luminosities of Ultraluminous Galaxies

Source	L'_{CO}	$M'(\text{H}_2)$	S_{25}	S_{60}	S_{100}	$\frac{S_{60}}{S_{100}}$	L_{FIR}	$\frac{L_{\text{FIR}}}{M'(\text{H}_2)}$	$\frac{L_{\text{FIR}}}{L'_{\text{CO}}}$
name	($10^9 L_l$)	($10^{10} M_{\odot}$)	(Jy)	(Jy)	(Jy)		($10^{12} L_{\odot}$)	$\frac{L_{\odot}}{M_{\odot}}$	$\frac{L_{\odot}}{L_l}$
00057+4021	3.8	1.7	0.36	4.47	4.30	1.04	0.31	17	80
00188–0856	6.7	3.1	0.37	2.59	3.40	0.76	1.51	48	224
00262+4251	6.2	2.9	0.33	2.98	2.44	1.22	0.99	34	160
I Zw 1	5.0	2.3	1.21	2.24	2.63	0.85	0.29	12	57
Mrk 1014	8.7	4.0	0.54	2.22	2.16	1.03	2.14	53	245
02483+4302	2.9	1.3	0.19	4.02	6.92	0.58	0.41	30	142
03158+4227	7.0	3.2	0.45	4.26	4.28	1.00	2.75	85	392
03521+0028	9.3	4.3	0.23	2.64	3.84	0.69	2.26	52	242
04232+1436	9.0	4.1	<0.38	3.45	4.26	0.81	0.75	18	83
VII Zw 31	11.8	5.4	0.58	5.58	9.62	0.58	0.64	11	53
07598+6508	11.4	5.2	0.53	1.69	1.73	0.98	1.34	25	118
08030+5243	8.8	4.1	0.18	2.99	4.39	0.68	0.75	18	85
08572+3915	1.3	0.6	1.70	7.43	4.59	1.62	1.00	166	766
09320+6134	4.7	2.1	1.03	11.54	20.23	0.57	0.69	32	148
10035+4852	7.0	3.2	0.28	4.59	6.24	0.74	0.67	20	94
10190+1322	8.2	3.8	0.38	3.35	5.57	0.60	0.75	19	91
10495+4424	8.2	3.8	0.16	3.53	5.41	0.65	1.12	29	136
10565+2448	5.6	2.6	1.14	12.12	15.13	0.80	0.76	29	135
11506+1331	7.5	3.4	0.19	2.58	3.32	0.78	1.47	42	196
Mrk 231	7.5	3.5	8.66	31.99	30.29	1.06	1.96	56	259
13106–0922	9.4	4.3	<0.36	1.66	2.42	0.69	1.89	43	201
Arp 193	3.8	1.8	1.36	15.44	25.18	0.61	0.31	17	81
Mrk 273	5.1	2.3	2.28	21.74	21.38	1.02	1.06	43	202
13442+2321	5.2	2.4	0.11	1.62	2.26	0.72	1.18	49	227
14070+0525	9.5	4.4	0.19	1.45	1.82	0.80	3.80	87	401

Table 2—Continued

Source name	L'_{CO} ($10^9 L_l$)	$M'(\text{H}_2)$ ($10^{10} M_{\odot}$)	S_{25} (Jy)	S_{60} (Jy)	S_{100} (Jy)	$\frac{S_{60}}{S_{100}}$	L_{FIR} ($10^{12} L_{\odot}$)	$\frac{L_{\text{FIR}}}{M'(\text{H}_2)}$ $\frac{L_{\odot}}{M_{\odot}}$	$\frac{L_{\text{FIR}}}{L'_{\text{CO}}}$ $\frac{L_{\odot}}{L_l}$
15030+4835	12.5	5.8	<0.08	0.90	1.46	0.62	1.70	29	135
Arp 220	7.0	3.2	7.91	103.80	112.40	0.92	1.16	35	164
16090–0139	12.2	5.6	0.26	3.61	4.87	0.74	2.29	40	188
16334+4630	9.5	4.4	<0.10	1.19	2.09	0.57	1.80	41	189
NGC 6240	7.9	3.7	3.42	22.68	27.78	0.82	0.45	12	56
17208–0014	7.1	3.2	1.66	34.14	34.90	0.98	2.14	65	302
18368+3549	8.5	3.9	<0.25	2.23	3.84	0.58	1.20	30	140
19297–0406	9.4	4.3	0.59	7.05	7.72	0.91	1.80	41	191
19458+0944	12.0	5.5	<0.28	3.94	7.11	0.55	1.59	28	132
20087–0308	16.1	7.4	0.24	4.70	6.54	0.72	1.87	25	116
22542+0833	6.0	2.8	<0.18	1.20	1.48	0.81	1.18	42	196
23365+3604	8.5	3.9	0.81	7.09	8.36	0.85	1.01	25	119
<i>median:</i>	8	—	—	—	—	0.8	1.3	35	160

$L_{\text{FIR}} = 3.94 \times 10^5 r(S_{60}/S_{100}) \cdot (2.58 S_{60} + S_{100}) D_L^2$, with L_{FIR} in L_{\odot} , S in Jy, D_L in Mpc, where $D_L = cH_0^{-1}q_0^{-2} \left\{ zq_0 + (q_0 - 1) \left[(2q_0z + 1)^{0.5} - 1 \right] \right\}$ (e.g., Weinberg 1972).

We adopt $H_0 = 75 \text{ km s}^{-1} \text{ Mpc}^{-1}$ and $q_0 = 0.5$.

$L_l \equiv \text{K km s}^{-1} \text{ pc}^2$, $M'(\text{H}_2) = 4.6 \cdot L'_{\text{CO}}$.

Table 3. Radii and Dynamical Masses Derived from CO Data

Source name	bb Temp. T_{bb} (K)	bb radius R_{bb} (pc)	CO radius R_{CO} (pc)	Dyn. Mass $M_{\text{dyn}}(< R_{\text{CO}})$ ($10^8 M_{\odot}$)	$\frac{M_{\text{dyn}}}{L'_{\text{CO}}}$ $\left(\frac{M_{\odot}}{L_l} \right)$	Density n_{tot} (cm $^{-3}$)
00057+4021	72	81	219	62	1.6	2850
00188–0856	62	238	297	105	1.6	1932
00262+4251	88	98	314	66	1.1	1023
I Zw 1	63	101	248	97	1.9	3060
Mrk 1014	80	174	418	87	1.0	576
02483+4302	50	197	273	57	2.0	1352
03158+4227	75	220	405	85	1.2	613
03521+0028	60	319	575	120	1.3	304
04232+1436	62	172	340	126	1.4	1544
VII Zw 31	50	244	616	129	1.1	265
07598+6508	76	153	377	99	0.9	893
08030+5243	56	208	345	141	1.6	1653
08572+3915	119	53	113	24	1.8	7862
09320+6134	49	266	295	84	1.8	1570
10035+4852	58	186	395	82	1.2	646
10190+1322	52	243	360	127	1.5	1316
10495+4424	55	265	379	96	1.2	846
10565+2448	59	188	317	66	1.2	1000
11506+1331	63	229	361	75	1.0	772
Mrk 231	73	198	378	79	1.0	702
13106–0922	61	281	496	104	1.1	410
Arp 193	50	170	244	95	2.5	3156
Mrk 273	70	157	280	59	1.2	1284
13442+2321	61	221	441	92	1.8	518
14070+0525	72	284	394	82	0.9	648

Table 3—Continued

Source name	bb Temp. T_{bb} (K)	bb radius R_{bb} (pc)	CO radius R_{CO} (pc)	Dyn. Mass $M_{\text{dyn}}(< R_{\text{CO}})$ ($10^8 M_{\odot}$)	$\frac{M_{\text{dyn}}}{L'_{\text{CO}}}$ $\left(\frac{M_{\odot}}{L_l}\right)$	Density n_{tot} (cm $^{-3}$)
15030+4835	59	281	499	104	0.8	404
Arp 220	64	197	270	144	2.1	3549
16090–0139	61	304	459	96	0.8	477
16334+4630	56	327	413	98	1.0	673
NGC 6240	59	146	341	108	1.4	1320
17208–0014	69	235	301	91	1.3	1602
18368+3549	53	299	396	100	1.2	775
19297–0406	68	222	385	80	0.9	680
19458+0944	51	373	465	132	1.1	633
20087–0308	59	297	466	173	1.1	824
22542+0833	67	182	436	91	1.5	529
23365+3604	63	191	372	83	1.0	777

$$T_{\text{bb}} \approx -(1+z) \left(\frac{82}{\ln(0.3 \cdot S_{60}/S_{100})} - 0.5 \right); \quad R_{\text{bb}} = (L_{\text{FIR}}/(4\pi\sigma T_{\text{bb}}^4)^{0.5} .$$

$$R_{\text{CO}}(\text{min}) = (L'_{\text{CO}}/(\pi T_{\text{bb}} \Delta V)^{0.5} ; \quad M_{\text{dyn}}(< R_{\text{CO}}) = 232 \cdot R_{\text{CO}} \cdot [\text{Max}(300, \Delta V)]^2 .$$

Table 4. Mass Estimates for Ultraluminous Galaxies

Source name	$M_{\text{dyn}}(< R_{\text{CO}})$ ($10^8 M_{\odot}$)	$M'(\text{H}_2)$ ($10^8 M_{\odot}$)	M_{thin} ($10^8 M_{\odot}$)	$100M_{\text{dust}}$ ($10^8 M_{\odot}$)
00057+4021	62	175	19	15
00188–0856	105	309	29	130
00262+4251	65	286	38	28
I Zw 1	97	230	22	22
Mrk 1014	87	402	48	76
02483+4302	57	133	10	82
03158+4227	85	322	37	115
03521+0028	120	427	38	207
04232+1436	126	413	38	61
VII Zw 31	129	544	41	111
07598+6508	99	523	60	57
08030+5243	141	406	34	44
08572+3915	24	60	11	46
09320+6134	84	214	16	26
10035+4852	82	324	28	119
10190+1322	127	378	30	88
10495+4424	96	376	31	168
10565+2448	66	258	23	82
11506+1331	75	345	33	148
Mrk 231	79	347	38	92
13106–0922	103	431	40	160
Arp 193	95	176	13	57
Mrk 273	59	230	25	56
13442+2321	92	239	22	106
14070+0525	82	435	47	188

Table 4—Continued

Source name	$M_{\text{dyn}}(< R_{\text{CO}})$ ($10^8 M_{\odot}$)	$M'(\text{H}_2)$ ($10^8 M_{\odot}$)	M_{thin} ($10^8 M_{\odot}$)	$100M_{\text{dust}}$ ($10^8 M_{\odot}$)
15030+4835	104	575	51	164
Arp 220	144	323	31	84
16090–0139	96	560	52	195
16334+4630	98	438	37	208
NGC 6240	108	366	33	44
17208–0014	91	325	34	123
18368+3549	100	393	31	171
19297–0406	80	434	44	107
19458+0944	132	552	42	261
20087–0308	173	740	66	184
22542+0833	91	277	28	101
23365+3604	83	390	37	77

Table 5. Optical / Near-IR Morphology of Ultraluminous Galaxies

Source name	Redshift cz (km s $^{-1}$)	Distance D_A (Mpc)	Morphology	Separation θ (arcsec)	$D_A \cdot \theta$ (kpc)	Ref.
00057+4021	13390	165	Double? disturbed	2.5 ?	2 ?	AHM87
00188–0856	38530	415	Merger + companion	7	14	M96
00262+4251	29153	330	Single	<0.8	<1.3	M96
I Zw 1	18330	220	Single (quasar)	—	—	
Mrk 1014	48947	501	Single (quasar)	—	—	
02483+4302	15419	188	Merger	3.8	3.5	KDBS
03158+4227	40296	431	Single	<0.8	<1.6	M96
03521+0028	45530	474	Double	1.6	3.6	M96
04232+1436	23855	278	Double, merger	4.6	5	
VII Zw 31	16260	196	Single (starburst)	—	—	
07598+6508	44621	466	Single (quasar)	—	—	HB89, S92
08030+5243	25031	290	Single	<0.8	<1.1	M96
08572+3915	17450	211	Double	6	5.5	S92
09320+6134	11785	147	Single; tails	<1.0	<0.7	S92, M96
10035+4852	19427	232	—	—	—	
10190+1322	22953	269	Double	5	6.6	Fig. 7
10495+4424	27674	315	Single, distorted	<0.7	<1.1	Fig. 7, M96
10565+2448	12923	160	Double, Multiple	8, 26	6, 20	Fig. 7, M96
11506+1331	38158	412	Double, Single	<0.5	<1.1	Fig. 7, M96
Mrk 231	12650	157	Double nucl.?, tail	3.5	2.8	A94
13106–0922	52290	526	Double	2	5	Fig. 7
Arp 193	7000	90	Single + 2 tails	>1 ?	>4 ?	S92
Mrk 273	11324	142	Double in NIR, 2 tails	0.9	0.6	M93
13442+2321	42620	450	Merger?	—	—	
14070+0525	79621	702	Single	—	—	Fig. 7

Table 5—Continued

Source name	Redshift cz (km s $^{-1}$)	Distance D_A (Mpc)	Morphology	Separation θ (arcsec)	$D_A \cdot \theta$ (kpc)	Ref.
15030+4835	64900	613	Double	3.5	11	Fig. 7
Arp 220	5450	70	Merger, double nuc.?	1	0.3	G90, M93, S94
16090–0139	40044	429	Single, distorted	<1.0	<2.2	Fig. 7, M96
16334+4630	57250	562	Double	4.4	12.6	Fig. 7
NGC 6240	7298	93	Double nucl.	—	—	AHM90; L94
17208–0014	12837	159	Double +tails, Single	<0.8	<0.6	Fig. 7, M96
18368+3549	34850	383	Single	<0.8	<1.5	M96
19297–0406	25700	297	Single	<1.9	<2.7	Fig. 7, M96
19458+0944	29980	338	Double?, Single	<0.8	<1.4	M96
20087–0308	31688	354	Single, tails	<1.0	<1.7	MM90, M96
22542+0833	49750	487	Double	—	—	
23365+3604	19330	231	Single, tails	<0.9	<1.1	Fig. 7, M96

$D_A = D_L/(1+z)^2$; for D_L , see footnote to Table 2.

A87, A90, A94: Armus et al. (1987; 1990; 1994); G90: Graham et al. (1990); KDBS: Kollatschny et al. (1991); L94: Lester & Gaffney (1994); M93: Majewski et al. (1993); M96: Murphy et al. (1996); MM90: Melnick & Mirabel (1990); S92: Sanders (1992); S94: Shaya et al. (1994).

Fig. 1.— Distribution of redshifts in our sample of ultraluminous galaxies.

Fig. 2.— CO(1–0) spectra of galaxies in our sample. The vertical scale is main-beam brightness temperature, in mK. Source names and redshifts are indicated in the boxes. For each source, the zero of the (Doppler) velocity scale is relative to the redshifts listed in Table 1. The spectra are in order of decreasing redshift.

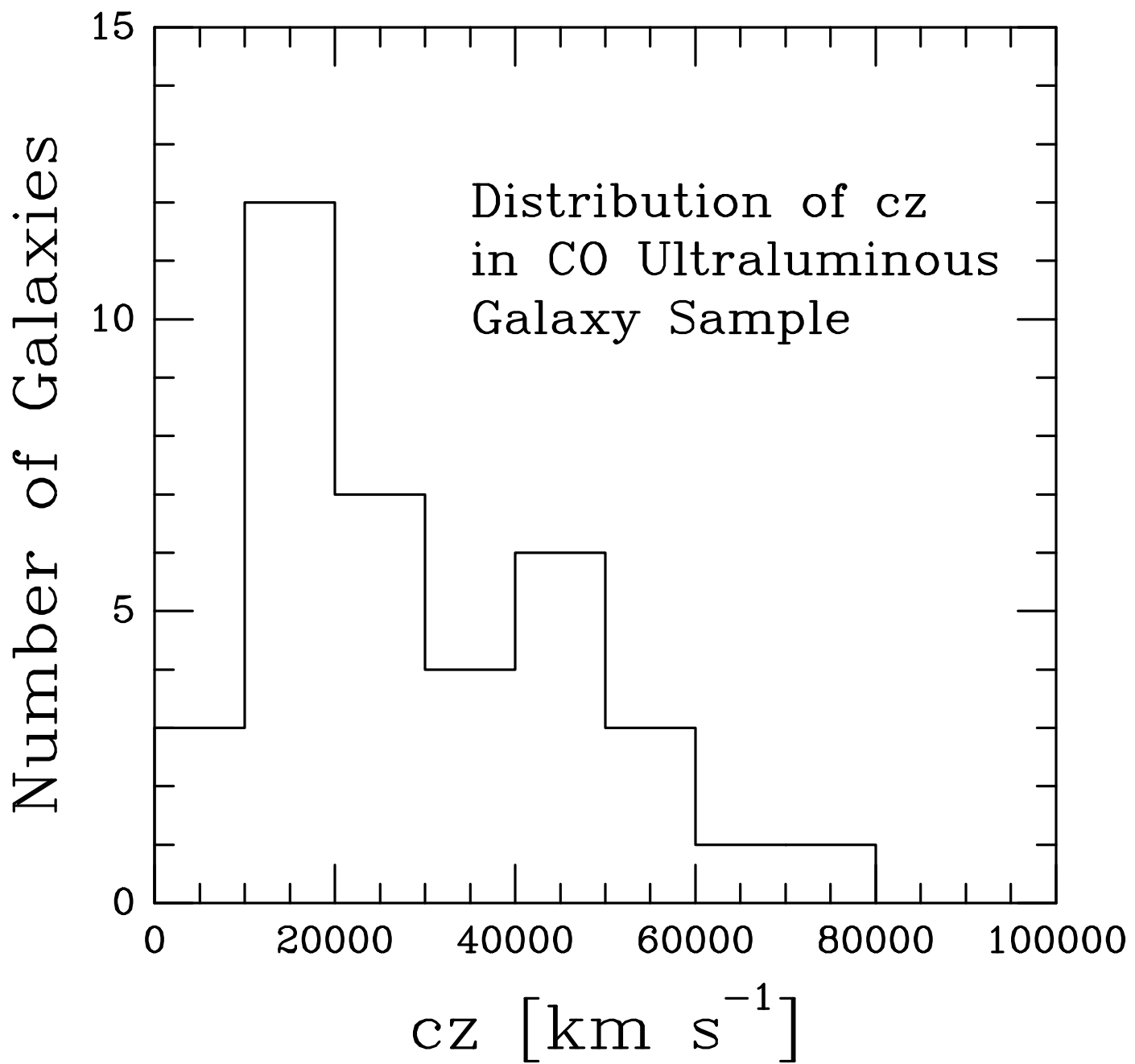
Fig. 3.— FIR luminosity vs. CO(1–0) luminosity (lower scale) and molecular gas mass (top scale). Solid circles indicate galaxies in our sample. Normal and weakly interacting spirals are scattered about the solid line. Open circles show locations in this diagram for some well-known galaxies.

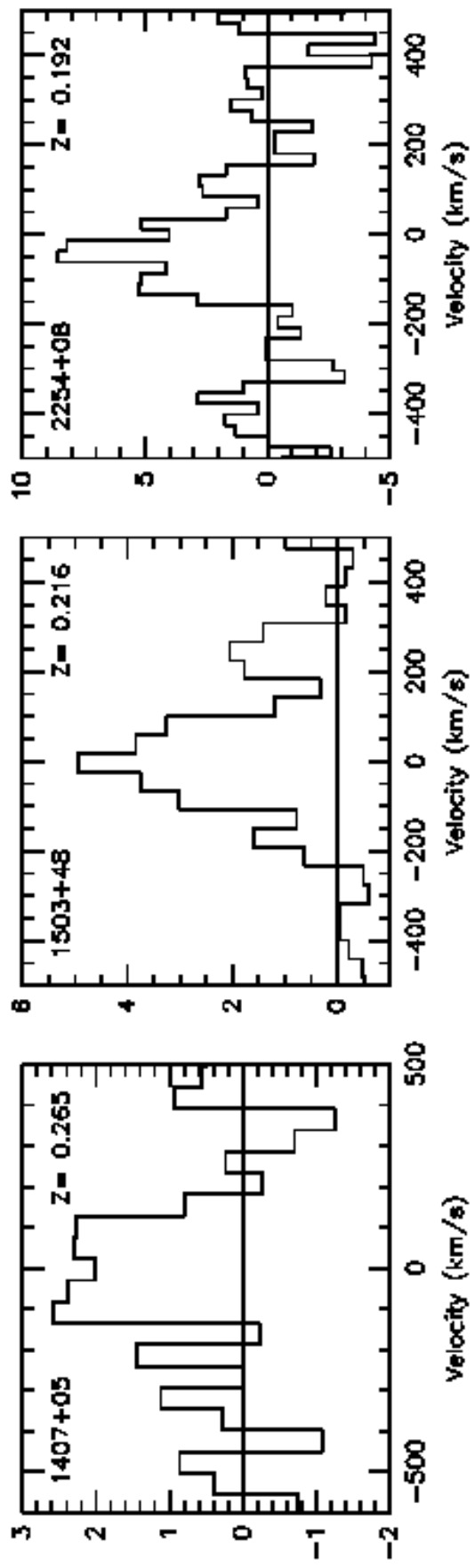
Fig. 4.— Integrated CO(1–0) line intensity, I_{CO} , in $\text{K}_{\text{mb}} \text{ km s}^{-1}$, vs. IRAS 100 μm flux density, in Jy, for the ultraluminous galaxies in our sample. The solid line corresponds to the relation $I_{\text{CO}} = 1.0 \times S_{100}$.

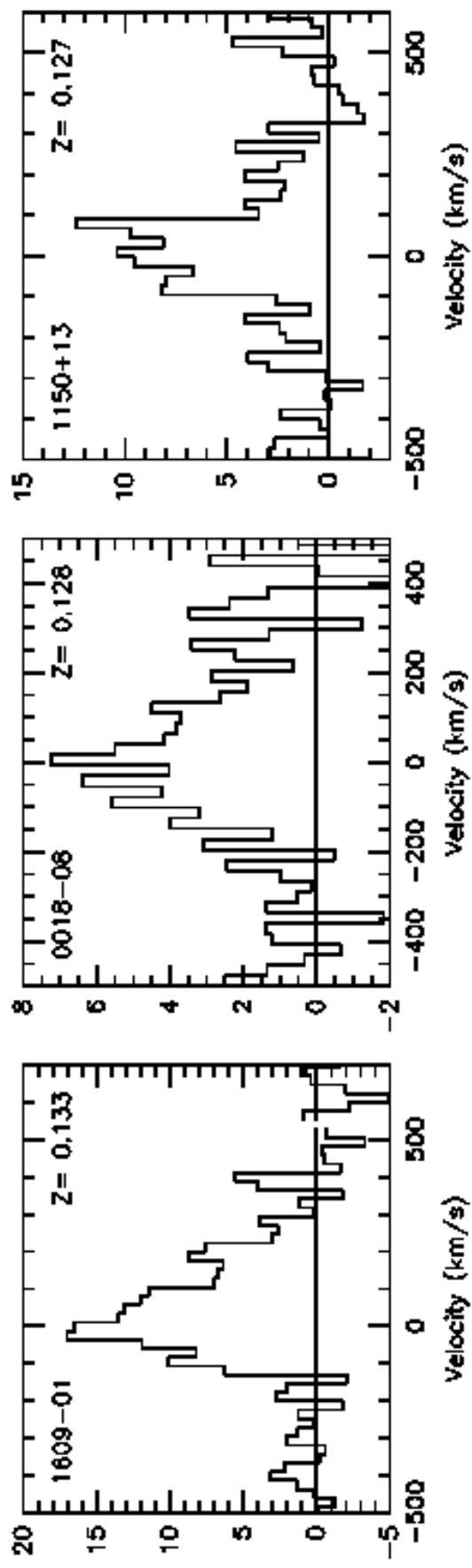
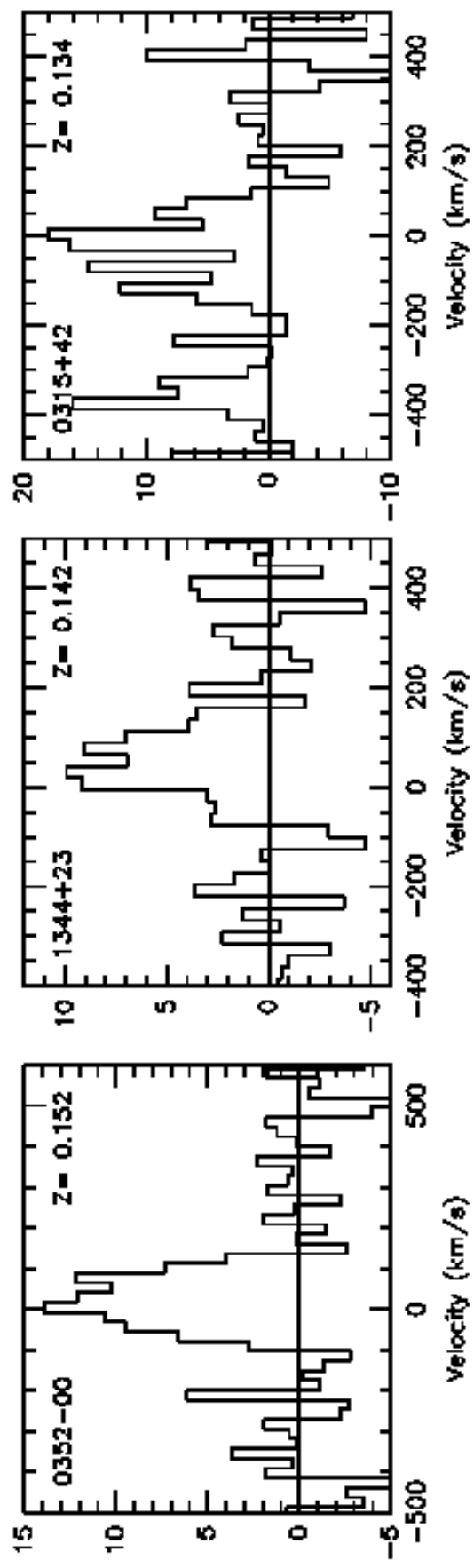
Fig. 5.— The distant-independent quantity $L_{\text{FIR}}/L_{\text{CO}}$ vs. the far IR black body dust temperature derived from the IRAS flux ratio S_{60}/S_{100} . The line indicates the upper limit for the luminosity ratio for the black body model in eq.(11), with $f_V \Delta V = 300 \text{ km s}^{-1}$. Solid circles: galaxies in our sample with $L_{\text{FIR}} > 10^{12} L_{\odot}$. Open circles: galaxies with $L_{\text{FIR}} < 10^{12} L_{\odot}$.

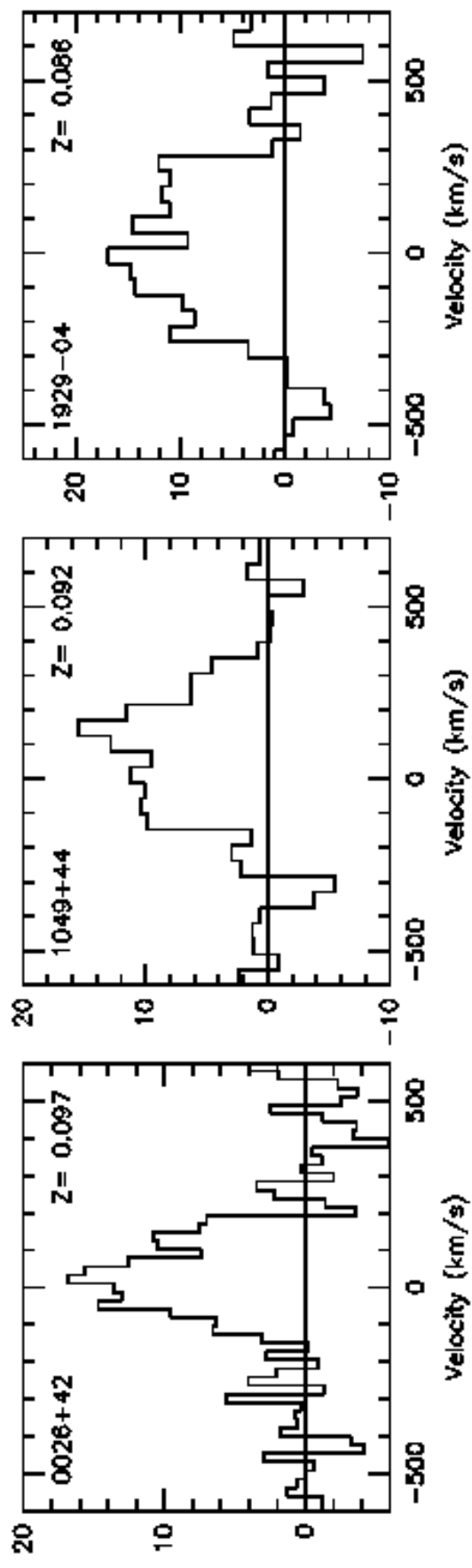
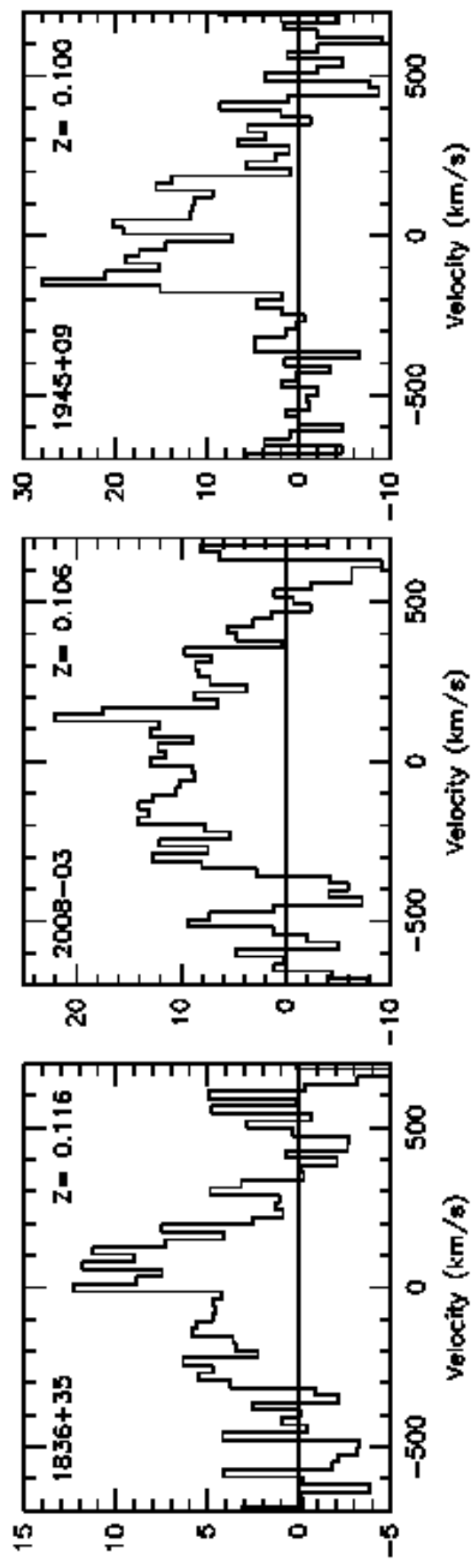
Fig. 6.— Distribution of observed CO full widths to half-maximum, ΔV , for the galaxies in our sample.

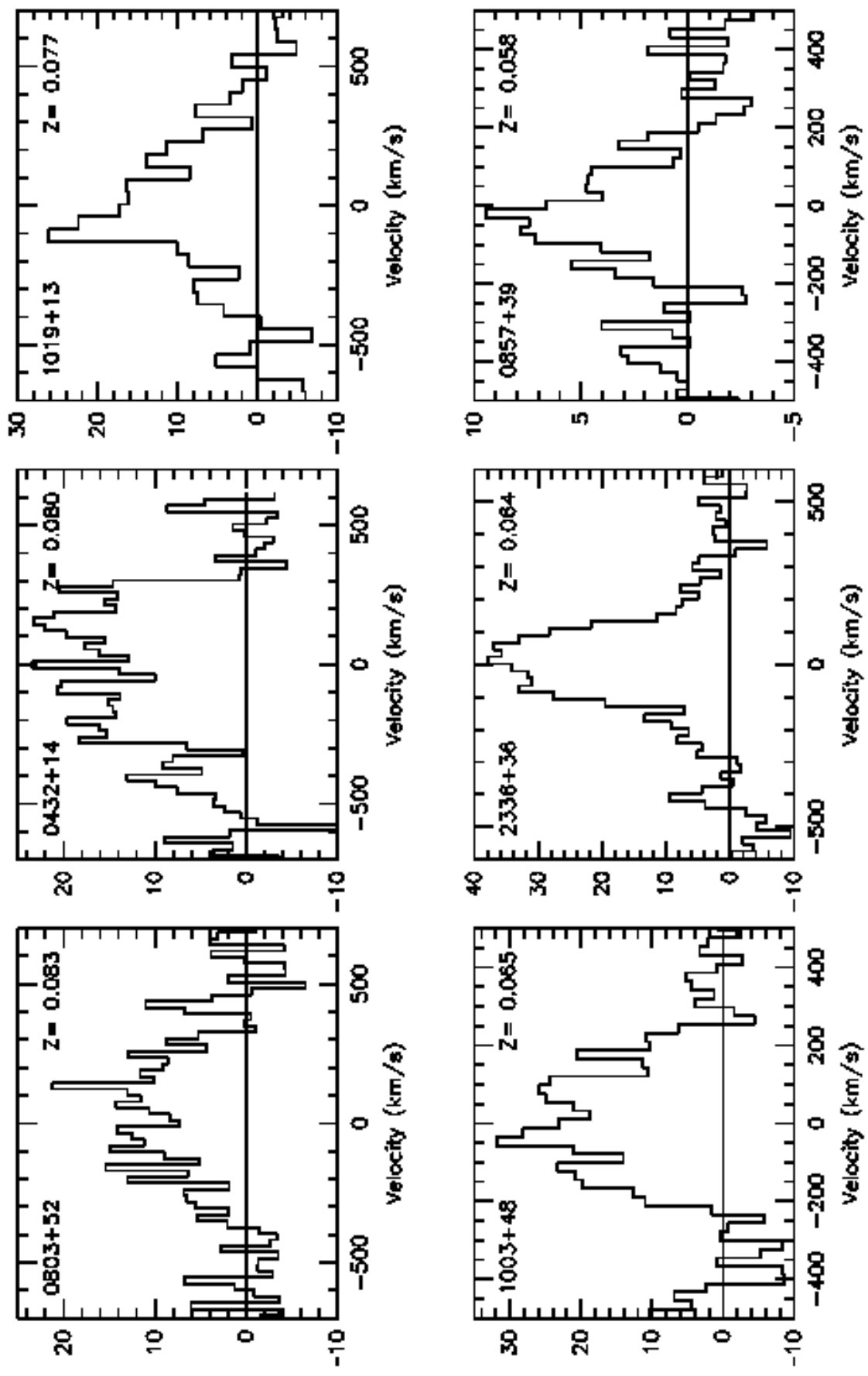
Fig. 7.— R-band CCD images of galaxies between RA 10h and 23h in the sample. The images are in order of decreasing redshift. North is at the top, east is to the left. Brightness contours are on an arbitrary linear scale. Next to each image is source name, redshift and CO(1–0) spectrum, with units as in Fig. 1. The images were taken at the Univ. of Hawaii 88-in. telescope by Sanders & Kim (1993, priv. communication).

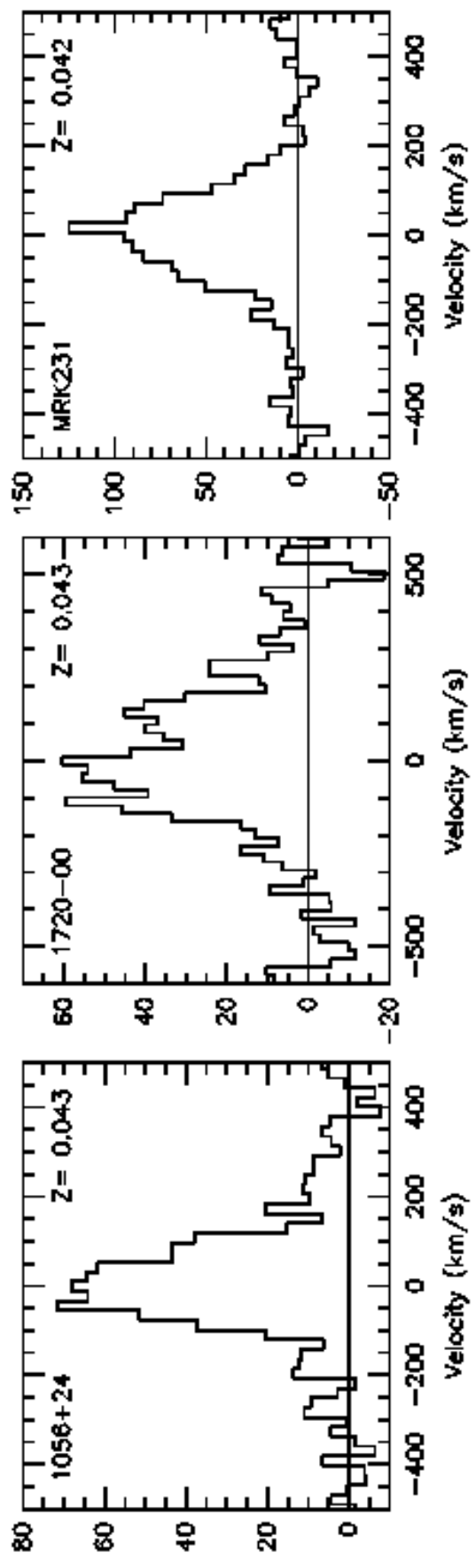
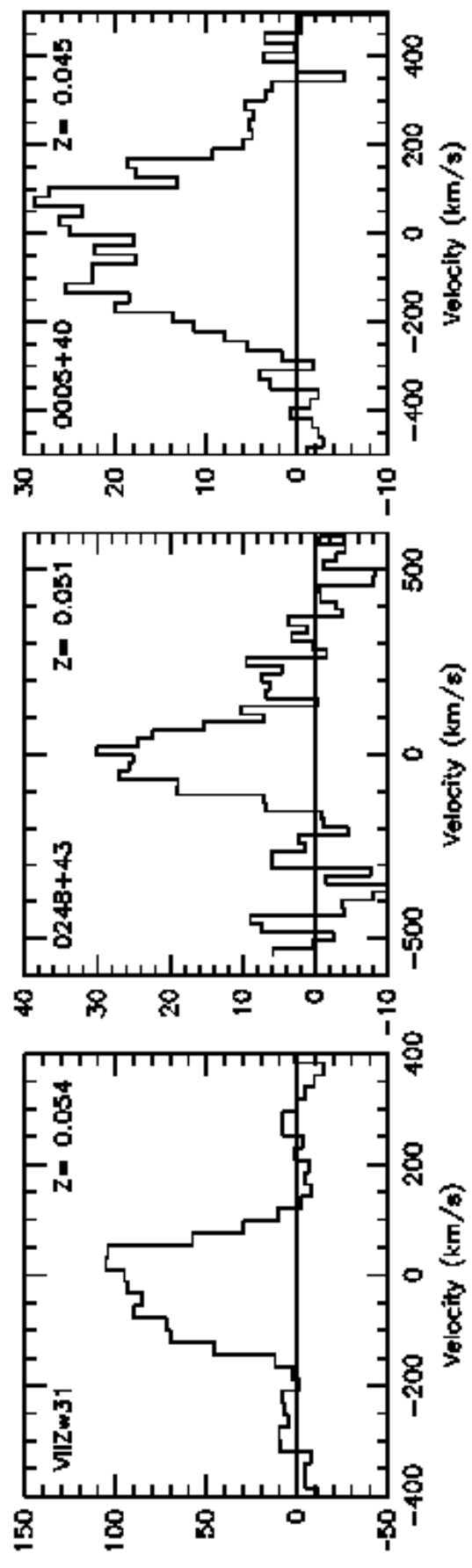


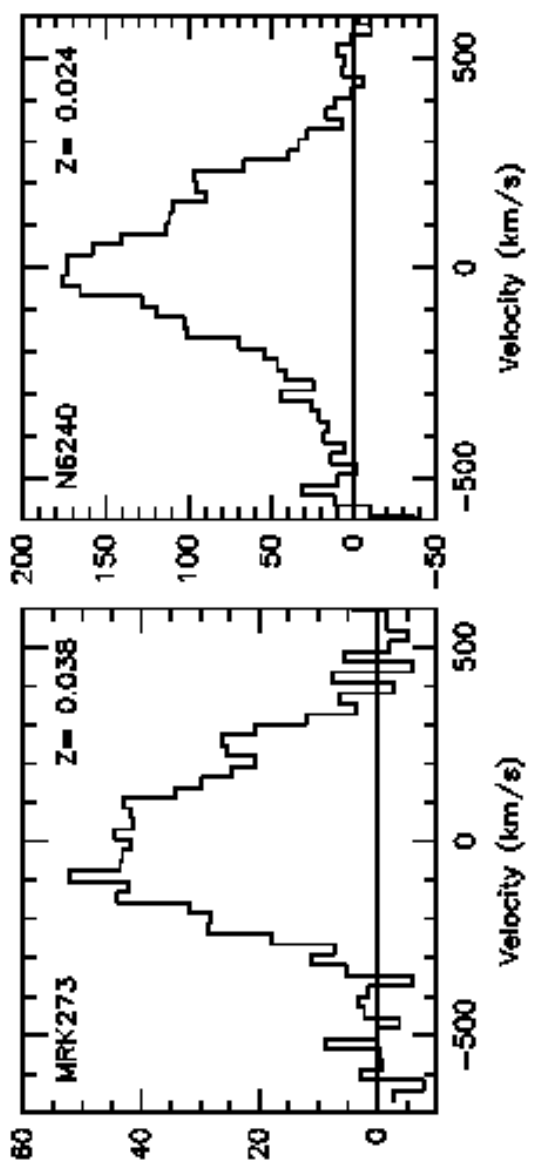
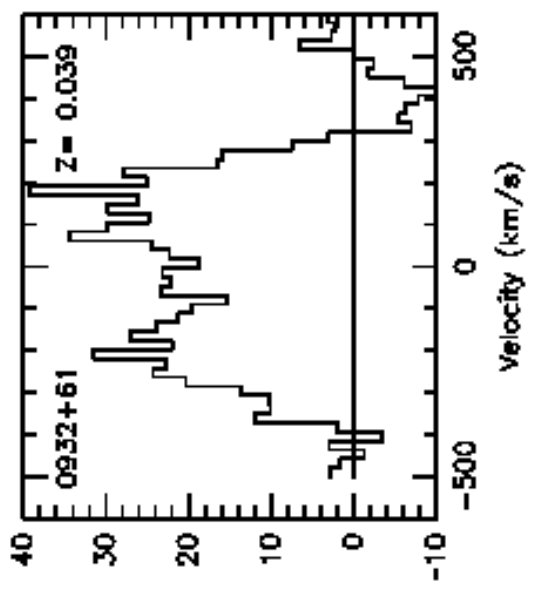
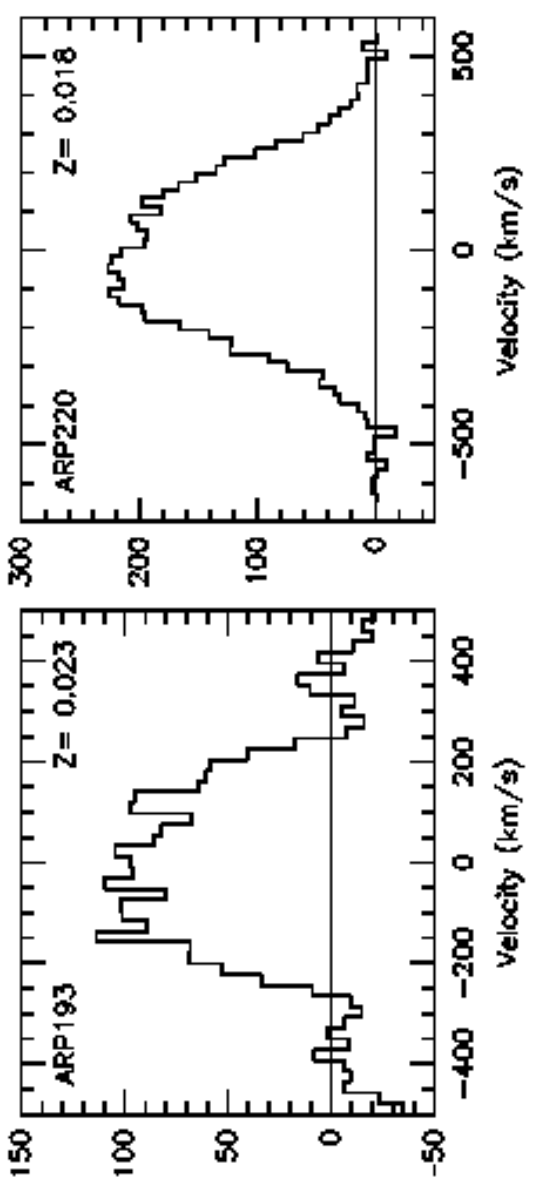
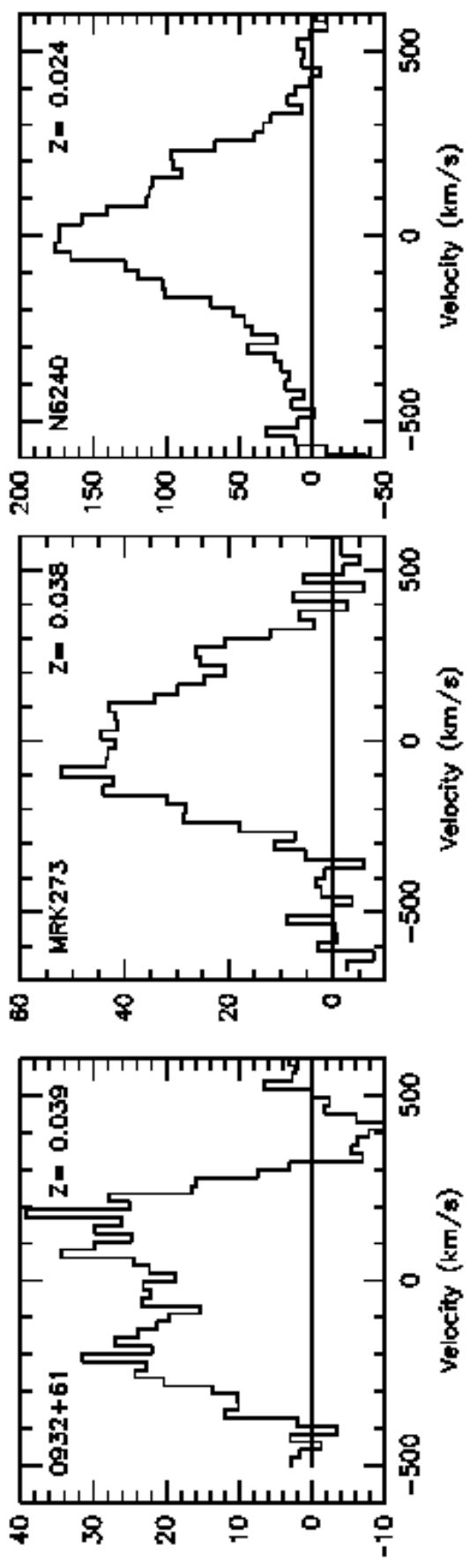


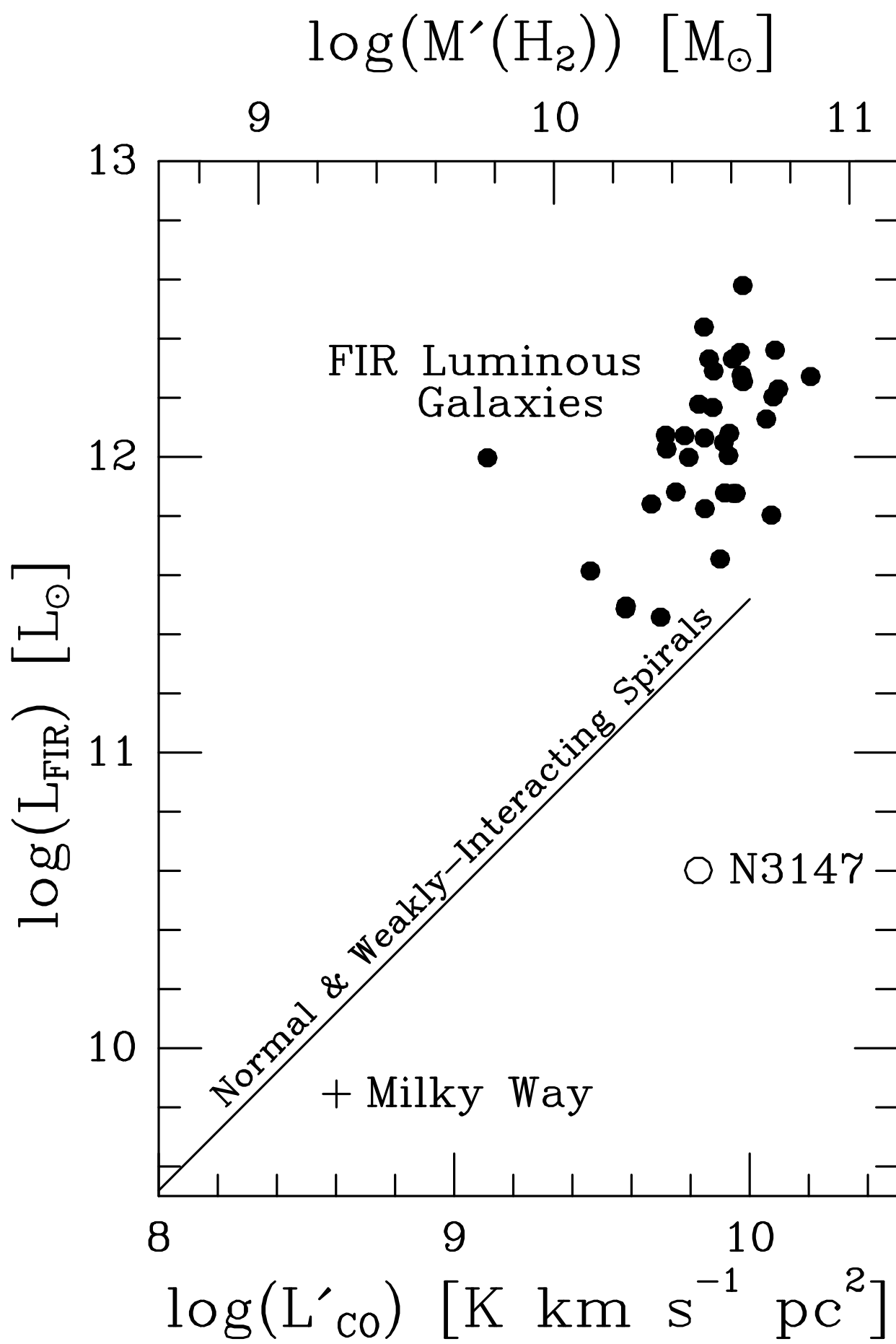


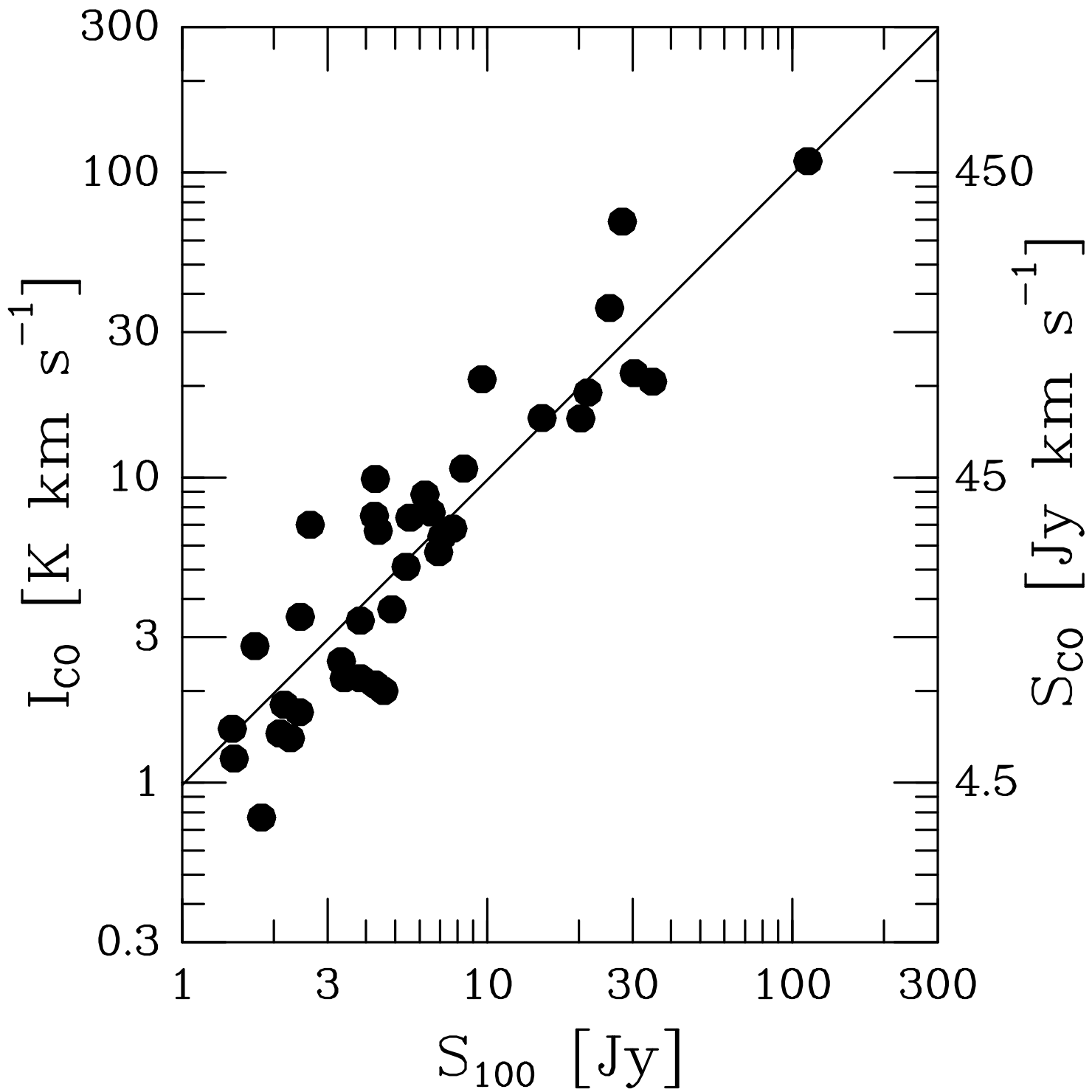


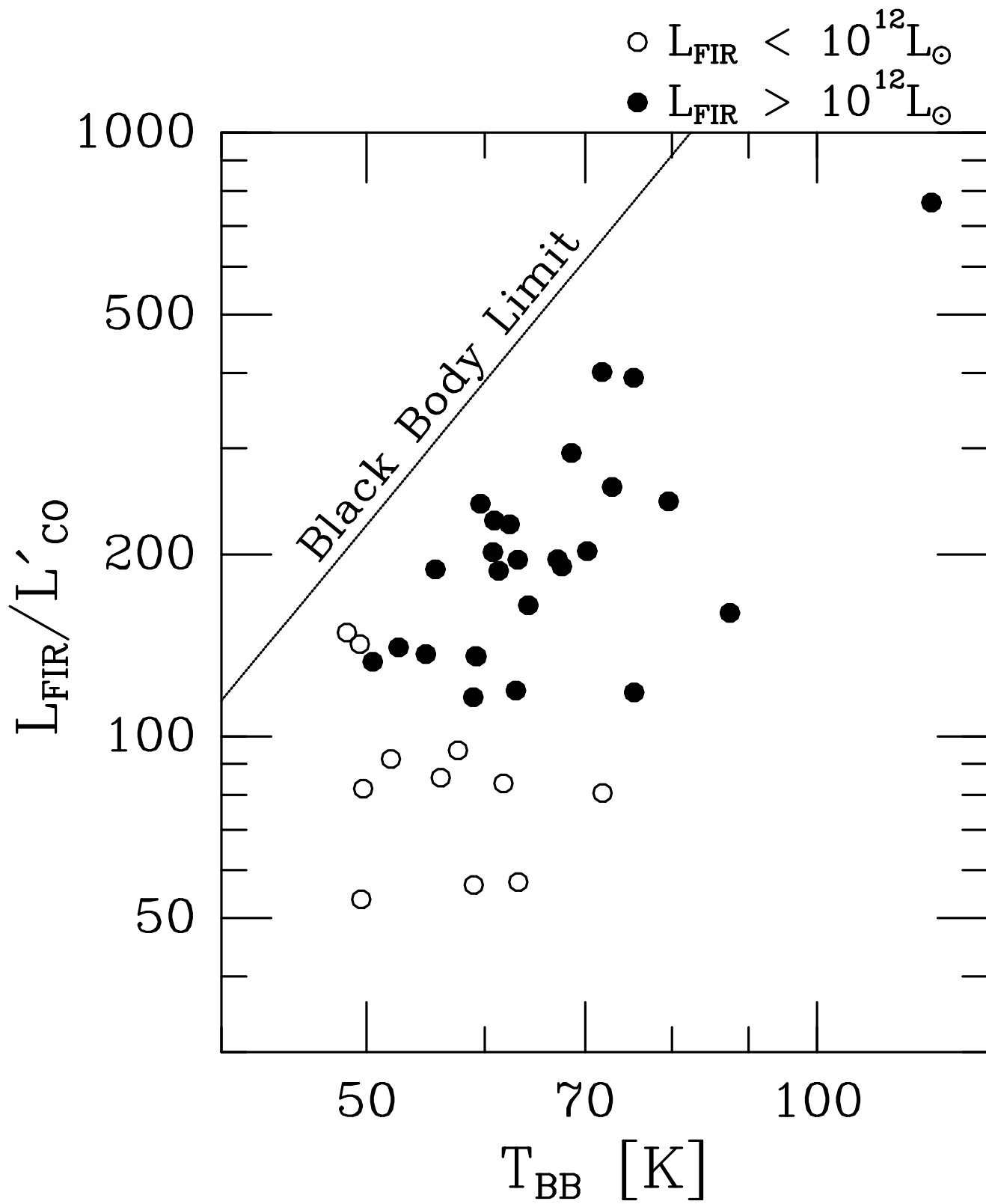


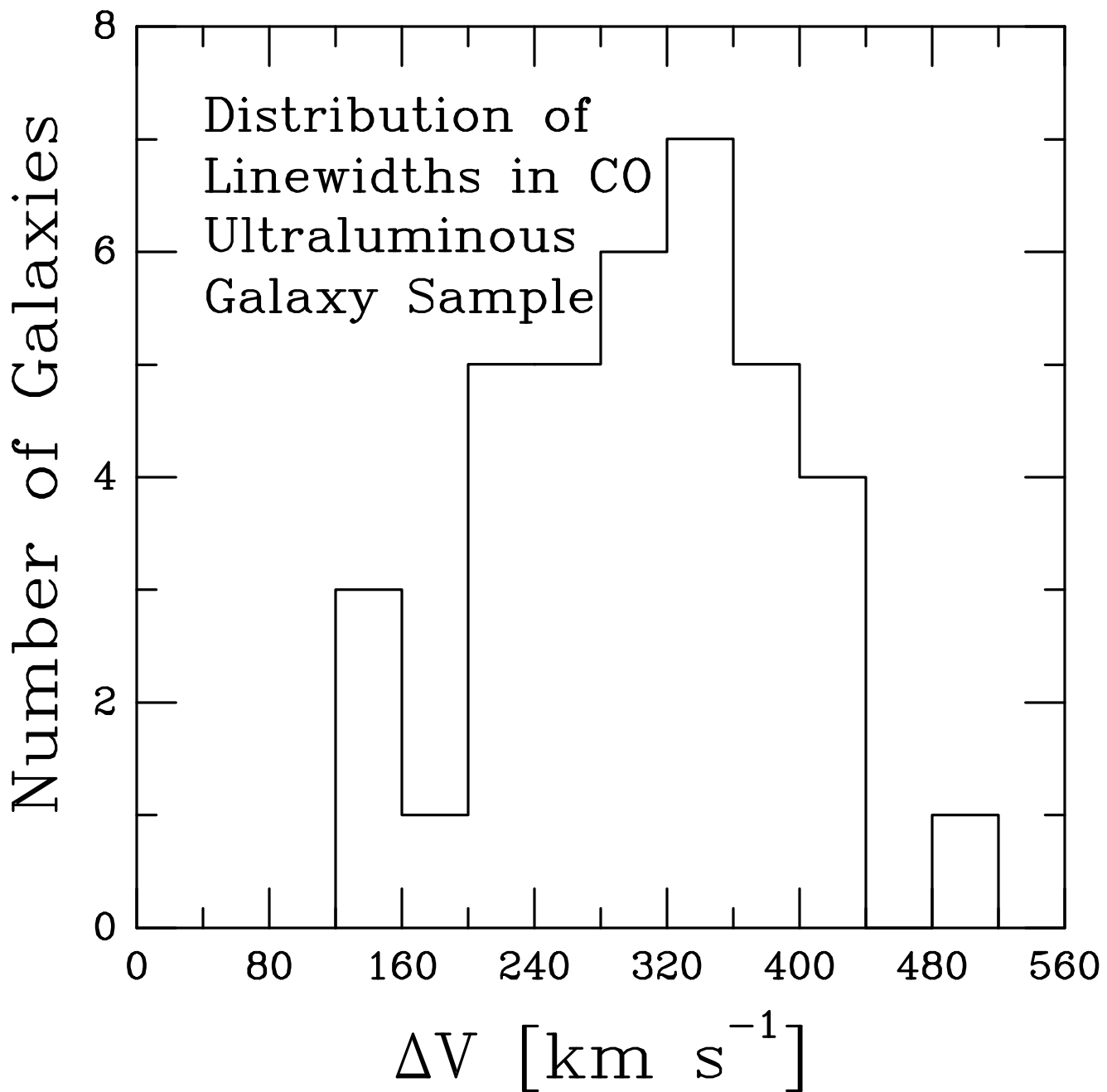








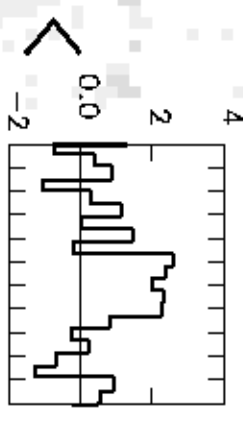




CO EMISSION FROM DISTANT ULTRALUMINOUS IR GALAXIES

■

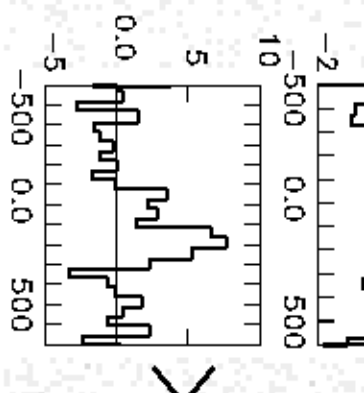
1407+05
 $Z=0.266$



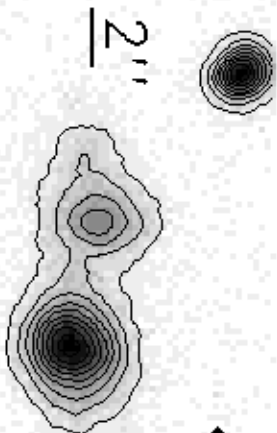
1503+48
 $Z=0.216$



1633+46
 $Z=0.191$

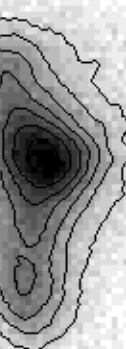


1310-09
 $Z=0.175$

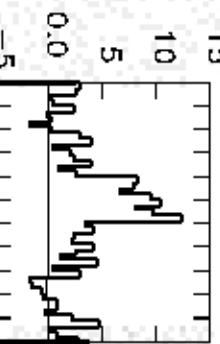
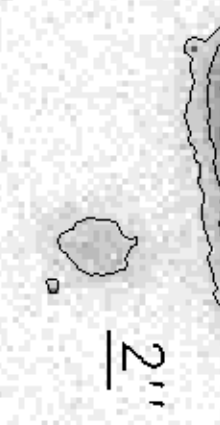


CO EMISSION FROM DISTANT ULTRALUMINOUS IR GALAXIES

1609-01
 $Z=0.134$

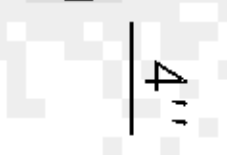
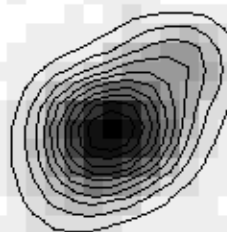
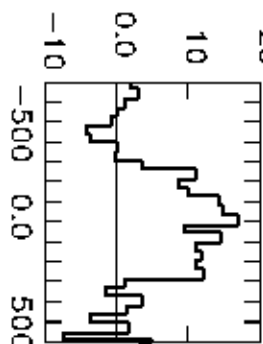
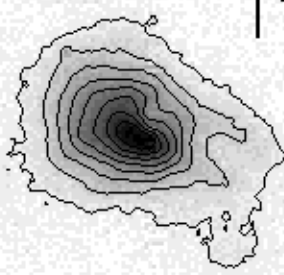


1150+13
 $Z=0.127$

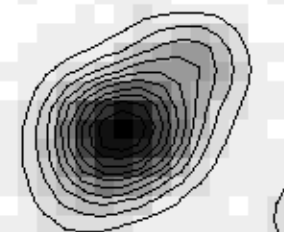


1049+44

$Z=0.092$

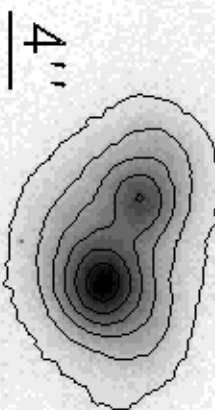


1929-04
 $Z=0.086$

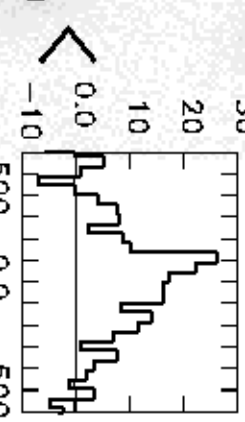


CO EMISSION FROM DISTANT ULTRALUMINOUS IR GALAXIES

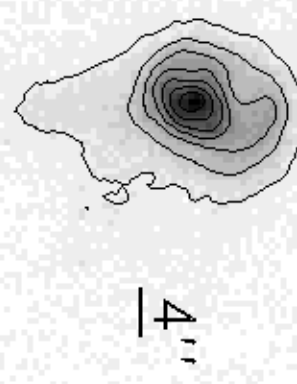
1019+13 $Z=0.077$



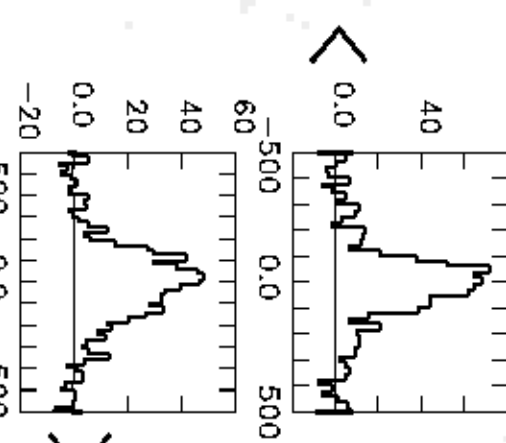
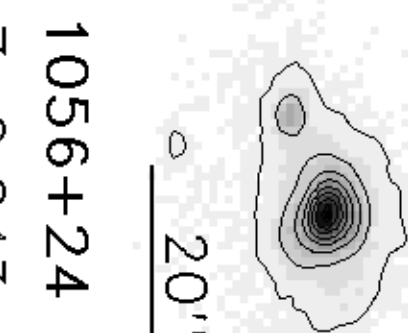
2336+36 $Z=0.064$



1720-00 $Z=0.043$



1056+24 $Z=0.043$



■